ASTRONOMY & ASTROPHYSICS
SUPPLEMENT SERIES

AUGUST **1999**, PAGE 213

Astron. Astrophys. Suppl. Ser. **138**, 213–245 (1999)

Multi-spectral study of a new sample of Blue Compact Dwarf Galaxies

II. *B* and *R* surface photometry of 22 southern objects⋆

V. Doublier[1,3], **A. Caulet**[3,4,5], **and G. Comte**[2]

[1] European Southern Observatory, Karl Schwarzschild St. 2, D–85748 Garching, Germany
[2] Observatoire de Marseille and Institut Gassendi, (CNRS), 2 place Le Verrier, F–13248 Marseille Cedex 04, France
[3] ST-ECF, European Southern Observatory, Karl Schwarzchild St. 2, D–85748 Garching, Germany
[4] Dept of Astronomy, University of Illinois at Urbana-Champaign, 1002 West Green Street Urbana, IL 61801, U.S.A.
e-mail: caulet@astro.uiuc.edu
[5] Previously affiliated to the Astrophysics Division, Space Science Department of the European Space Agency

Received January 22, 1998; accepted May 25, 1999

Abstract. We present the results of surface photometry on a new sample of Blue Compact Dwarf galaxies (BCDGs), in continuation to a previous paper (Doublier et al. 1997, hereafter Paper I). The 22 galaxies (plus two companions) discussed in the present paper have been selected in the Southern Hemisphere, from several lists. An atlas containing isophotal maps, surface brightnesses and $B-R$ color profiles of the sample is given, together with the tables containing the photometric parameters.

The results are consistent with those obtained in Paper I for objects selected from the Byurakan Surveys in the Northern hemisphere. Similarly, we find about one fourth of the BCDGs showing a dominant $r^{1/4}$ brightness distribution component, one fourth of the BCDG showing a dominant exponential surface brightness profile, and about half of them show composite brightness distributions. Integrated properties, colors, mean surface brightnesses and luminosity-radius relations are investigated and discussed for the objects presented in this paper and Paper I. We found that $r^{1/4}$ BCDGs tend to show a different behaviour compared to the exponential BCDGs, with respect to colors, compactness and luminosity-radius relations. We also include a brief study of the surroundings of the galaxies, where we find several candidate companions.

Key words: galaxies: compact — galaxies: photometry — galaxies: starburst — galaxies: structure

Send offprint requests to: V. Doublier

⋆ Based on observations collected at the 1.54 m Danish Telscope at the European Southern observatory (La Silla, Chile).

1. Introduction

Blue Compact Dwarf galaxies present striking properties, a UV-excess in the continuum produced by a very young integrated stellar population, as well as a strong nebular emission spectrum similar to H II regions. (Terlevich et al. 1991; Storchi-Bergmann et al. 1995). The generally high surface brightness of their star-forming regions and their small intrinsic sizes have led observers to call them "compact" objects. Low luminosity (dwarf) systems have absolute magnitudes fainter than −18 (Thuan & Martin 1981) or −16.5 (Zwicky 1971), depending on the luminosity cutoff arbitrarily defined by the authors, and extending to −12. BCDGs appear to have little dust and low metallicity compared to giant starburst galaxies (from 1/6 to 1/50 $Z_{\odot}$, Kunth & Sargent 1986; Thuan et al. 1997). They are experiencing a strong star formation episode that will exhaust their gas content in a few 10^8 years if no replenishment occurs.

Hypothetical evolutionary schemes (Burkert 1989; Kruger et al. 1994) place them between the slowly evolving gas rich Magellanic dwarf irregulars (dIs) and evolved gas-free dwarf ellipticals (dEs), implying that dIs could be the quiescent phase of the BCDGs, and dEs the evolved results. More recently, Sung et al. (1998) have argued that BCDGs and dEs have similar intrinsic shapes, i.e. their axis ratios show a similar distribution. Although this assumption presents the advantage of drawing an unified scheme of the evolution of low luminosity galaxies, it is still confronted with serious problems related to the differences in light distribution and dynamics between the three classes of dwarfs (Van Zee et al. 1998).

Early studies by Loose & Thuan (1986a and b), and Kunth et al. (1988) have shown that the morphology of BCDGs varies greatly from galaxy to galaxy. From morphology considerations, Loose & Thuan (1986b) have proposed the following classification where a large majority is composed of analogs to the quiescent dwarf ellipticals and dwarf irregulars, *a*- with regular isophotes like elliptical dwarf galaxies (dE), *b*- with a bright central star forming region like the nucleated dE (n, dE), *c*- with very irregular isophotes like the dwarf irregulars (iI, with cometary (C), and merger (M) as peculiar subdivisions). Finally, a small fraction of the BCDGs have been classified as i0-BCDGs because they are unresolved without detected low surface brightness underlying compoment.

This morphological classification has been proposed regardless of a quantitative determination of the surface brightness distribution whereas the dynamics of the starburst and its host galaxy need detailed investigations.

Recent photometric studies have shown that the BCDGs appear to follow a somewhat simpler classification: in our previous paper, (Paper I) we report that among the 23 BCDGs observed, 1/3 are classified as spheroidal analogs (showing $r^{1/4}$ law dominated light profiles), 1/3 are classified as exponential law dominated galaxies, and 1/3 have composite light profiles. The fact that these galaxies have similar components as normal giant galaxies suggests that they may have a similar dynamical history, related to their star formation history. Dynamically, BCDGs seem to be complicated systems, as suggested by detailed surface photometry (Papaderos et al. 1996a; Telles et al. 1997; Telles & Terlevich 1997). Some BCDGs present signatures of interactions and merging, although very few are known to have companions or to be found in close groups (Pustil'nik et al. 1995).

Our goals are to study the intrinsic properties of BCDGs derived from their light distribution and their structure; we have searched for the areas of star formation, for the presence of disks, spheroids, or non-axisymmetric components, for traces of possible interactions, and for color gradients. Also, we have searched for relationships between the photometric parameters and the spectroscopic indicators of galactic evolution (e.g. the metallicity of the ionized gas, the ages of the starburst and its possible host galaxy); finally, we have studied the environment of the BCDGs by searching for interacting neighbours (galaxies or clouds). This paper presents the results of the second part of the imaging and photometric observing program at visible wavelengths, whose first part was reported in Paper I. This program is coupled to another one at high spectral resolution, using multi-pupil spectroscopy, of the continuum and emission lines of BCDGs. Near-infrared images of the BCDGs presented in this paper have also been obtained (Doublier et al. 1999, in preparation).

2. The sample

In the following, we describe results from B and R imagery on a new sample of 22 objects selected from several Southern Sky catalogs. Our interest residing in compact H II galaxies, we selected objects at low redshift (typically smaller than 2000 km s^{-1}), with estimates of absolute magnitudes $M_b \geq -17$ using the same selection criteria as for the objects described in Paper I.

Ten objects in the present work come from the Tololo sample (Smith et al. 1976; Bohuski et al. 1978) and three from the University of Michigan (UM) survey (MacAlpine & Lewis 1978; MacAlpine et al. 1977 and MacAlphine & Williams 1981). We also used both Tololo and UM surveys with good spectroscopic follow-up (Salzer et al. 1989a; Terlevich et al. 1991). Three objects come from Zwicky's southern lists, investigated by Rodgers et al. (1978), and four objects come from Fairall's list of compact galaxies (Fairall 1977; Fairall 1981), recognized as HII galaxies by follow-up spectroscopy; among these, two were already in the Tololo lists. The galaxy 13209−2723 has been found by Surace & Comte (1997) in an objective-prism survey conducted with the ESO 1 m Schmidt telescope, described in Surace & Comte (1994). Haro 14 and the well-known compact Mk 600 have been added to the list. Finally, Mk 996 has been re-observed because of the apparent inconsistency of the results of Paper I with those derived by Thuan et al. (1996) with the Hubble Space Telescope. UM 465 has been also re-observed in order to be able to derive the surface photometry of its small companion (UM 465B, see Paper I).

Table 1 lists the observed galaxies. The apparent magnitudes are the estimated magnitudes given in the original lists.

3. Observations and data reduction

3.1. Observations

The observations were made at the Southern European Southern Observatory (La Silla, Chile) by Doublier and Caulet using the 1.54 m Danish Telescope, during two periods: April 29 - May 3 and December 20-23, 1995. In April-May, the direct camera was equipped with a thinned back-illuminated 1024×1024 pixel Tektronix CCD (ESO #28) with a pixel scale of 0.36″. In December, DFOSC (Danish Faint Object Spectrograph and Camera) was equipped with the thinned Loral 2048×2048 CCD#17 with a pixel scale of 0.38″.

Each galaxy field was exposed three times with a dithering step equal to at least the size of the galaxy in order to correct for blemishes on the CCD chip. Short exposures were taken to avoid saturation of bright stars in the fields that could create ghosts and uneven background, CCD saturation and bleeding. The data were bias

Table 1. List of selected objects

Object	α(2000)	δ(2000)	$v_{\rm rec}$ (km s^{-1})	app. mag. (V)	Observation period
Haro 14	00 45 46	−15 35 37	970	13.9	Dec. 1995
Mk 996 (*)	01 27 35	−06 19 36	1634	15.5	Dec. 1995
UM 417	02 19 30	−00 58 57	2663	18.2	Dec. 1995
Mk 600	02 51 41	04 27 09	1010	14.8	Dec. 1995
Fairall 301	04 06 07	−52 40 11	679	14.3	Dec. 1995
Tol 0513−393	05 15 19	−39 17 41	14368	14	Dec. 1995
Tol 0610−387	06 12 13	−38 46 25	1505	15	Dec. 1995
Tol 0645−376	06 46 50	−37 43 21	7321	16	Dec. 1995
Tol 0954−293	09 56 14	−29 37 17	1839	16	Dec. 1995
Tol 0957−279	09 59 21	−28 07 24	420	15.1	Dec. 1995
Tol 3 (**)	10 06 32	−29 56 08	865	13.6	Dec. 1995
Fairall 6 (***)	11 11 06	09 37 53	1911	16	Apr./May 1995
UM 461	11 51 32	−02 22 22	311	16.4	Apr./May 1995
UM 465 (*)	11 54 11	00 08 18	909	14.2	Apr./May 1995
I SZ 59	11 57 27	−19 36 41	1521	14	Apr./May 1995
I SZ 399	12 19 59	−17 23 38	683	15	Apr./May 1995
II SZ 34	13 19 28	−15 07 44	2608	16	Apr./May 1995
13209-2723	13 23 45	−27 39 36	2388	15.5	Apr./May 1995
Tol 1434+032	14 37 19	03 03 01	1291	15.8	Apr./May 1995
Tol 1448+116	14 50 36	11 24 39	1843	14.5	Apr./May 1995
Tol 1924−416	19 27 57	−41 34 31	2780	13.3	Apr./May 1995
Tol 1937−423	19 40 39	−42 12 15	2608	15.4	Apr./May 1995

(*): Already observed in Paper I.
(**): Or Tol 1004−296.
(***): Or Tol 1108+098.

subtracted, flat fielded and combined in the standard way, using the IRAF package.

During both runs, the weather was clear, and the seeing was between 0.9 and 1.1″ ($FWHM$ measured on field stars close to the objects). Weather conditions did not vary much during the nights, the variations of airmass-dependent terms in Eqs. (1) and (2) were less than 0.005. In addition, we observed the galaxies close to meridian, to reduce the variation of atmospheric absorption. Therefore, seeing and/or absorption were not important effects when we combined the frames, even those taken during different nights.

We used Johnson B and R ESO filters in combination with the CCDs, producing instrumental systems that are easy to convert to the standard Cousins system. The color terms were found to be negligible for both filters. For the photometric calibration, some Landolt (1992) equatorial standard stars were followed throughout the nights at different airmasses. Table 2 summarizes the observation log, as well as the signal-to-noise ratio obtained at the surface brightness of 25 mag/arcsec^2 in both bands.

3.2. Standard stars

Aperture photometry was performed on standard Landolt stars. We obtained the following equations which are used to convert our instrumental magnitudes (b, r) and colors to the Johnson-Cousins system, the values in parenthesis correspond to those obtained during the December run:

$$B = b_{\rm April,(December)} - 0.27 \times {\rm airmass} + 22.60(22.70) \quad (1)$$

$$R = r_{\rm April,(December)} - 0.09 \times {\rm airmass} + 23.35(23.65) \quad (2)$$

$$b = -2.5 \times \log\left(F_{b,\rm cor}\right) \quad (3)$$

$$r = -2.5 \times \log\left(F_{r,\rm cor}\right) \quad (4)$$

where $F_{b,\rm cor}$ and $F_{r,\rm cor}$ are the sky subtracted fluxes in counts per second, in B and R bands respectively.

The atmospheric absorption coefficients and zero points magnitudes were determined each night in a standard way. The values given in the above equations are average values for each observing period.

The Johnson R filter includes the H_α emission line in the rest frame; all objects have low redshift, and their H_α emission is always included in the measured R flux. Over the galaxy, the H_α flux is less important than a substantial background from an evolved stellar population, but it may, in some cases, produce a local red excess inside the galaxies, especially in star forming complexes that may have a large equivalent width of H_α emission.

Table 2. Observing log

object Name	Color Band	Exposure time (min)	S/N (25) B, R
Haro 14	B & R	2×10, 2×5	13 & 11
Mk 996	B & R	2×10, 2×5	12 & 13
UM 417	B & R	2×10, 2×5	10 & 11
Mk 600	B & R	2×10, 2×5	16 & 17
Fairall 301	B & R	2×10, 2×5	11 & 12
Tol 0513−393	B & R	2×10, 2×5	9 & 13
Tol 0610−387	B & R	2×10, 2×5	13 & 12
Tol 0645−376	B & R	2×10, 2×5	12 & 12
Tol 0954−293	B & R	2×10, 2×5	12 & 13
Tol 0957−279	B & R	2×10, 2×5	12 & 15
Tol 3	B & R	2×10, 2×5	13 & 14
Fairall 6	B & R	5×8, 4×3	10 & 7
UM 465	B & R	4×10, 3×5	13 & 9
UM 461	B & R	3×10, 3×7	12 & 13
I SZ 59	B & R	4×8, 6×4	10 & 7
II SZ 34	B & R	5×10, 4×5	13 & 8
I SZ 399	B & R	4×8, 4×3	10 & 6
13209-2723	B & R	3×10, 4×3	12 & 5
Tol 1434+032	B & R	5×10, 5×5	13 & 9
Tol 1448+116	B & R	4×10, 3×10	14 & 19
Tol 1924−416	B & R	3×10, 5×4	11 & 7
Tol 1937−423	B & R	3×10, 4×5	8 & 9

$S/N(25)$: Signal to noise ratio at $\mu = 25$ mag/arcsec^2.

3.3. Galaxy photometry

3.3.1. Data reduction

The surface photometry of the galaxies was done with our own MIDAS (see Paper I) macro-procedures, and the reader is referred to Paper I for a complete description of the methods used. We briefly summarize the method: an isophotal integration of the flux was done without setting any constrain on the geometry of the isophotes (equivalent profile method, De Vaucouleurs 1959; Fraser 1977). After a careful estimation of the local sky background, the following photometric parameters were derived (using the notation from De Vaucouleurs 1959): the equivalent radius $r_{\rm eff}$ and $r_{0.25}$, within which are contained half and a quarter of the total luminosity respectively; they were derived from the curve of growth of the instrumental magnitudes, before Galactic foreground extinction correction. The asymptotic magnitude was extrapolated from the last 4 points on the integrated magnitude curve of growth. The surface brightnesses at $r = r_{\rm eff}$ and $r_{0.25}$, and the average surface brightness inside the effective radius, $< \mu_{\rm eff} >$, were also measured. We have checked that the variation of the derived parameters with different values of extinction is not large, considering the errors on the measurement of the radius, and the estimation of the asymptotic magnitude. For instance, adding an arbitrary value of $A_B = 0.3$ mag to the galaxy leads to decrease the effective radius by 0.2 arcsec. This is not significant considering the average seeing of $1.1''$ we had throughout our runs.

The sky background was checked to be flat in the vicinity of the objects. Since our procedures to derive the surface photometry take into account the local sky background, we wanted to avoid sky background subtraction on the image. In the cases of sky gradients under the objects, we subtracted a two-dimensional fit of the sky from the images.

As in Paper I, to increase the signal-to-noise ratio of the faint outermost isophotes, we have performed the isophotal integration in two steps. First, we used the direct image to produce a surface brightness profile, valid at bright intensity levels, then we smoothed the images with a Gaussian filter of a few pixels of width that matched the seeing disk of the images, and we built a second profile. Finally, the two surface brightness profiles were merged.

3.3.2. Errors

The errors in magnitudes and surface brightness were estimated assuming Poisson statistics, and taking into account the errors on the sky background estimation (based on local 1-σ variation). We used the relation given by Saglia et al. (1997).

The errors on the asymptotic magnitudes are more difficult to estimate accurately because pure Poisson statistics do not apply, and due to the extrapolation of a

magnitude based on the last four points of the photometric profile. We estimate that the errors are of the order of those made on the photometric calibration, e.g. 1%.

3.3.3. Photometric results

The results of the photometry are presented in Fig. 1 and Table 3. For each galaxy, Fig. 1 shows the isophotal map in B, the surface brightness distribution in the B and R bands, and the $B-R$ distribution. The orientations are from Haro 14 to Tol 3 North to the top and East to the left, and from Fairall 6 to Tol 1937−423 North down and East right. Table 3 collects the observable parameters derived from the photometry.

The data in Table 3 have not been corrected for Galactic foreground extinction. Extinction has been applied when deriving the integrated parameters such as the absolute magnitudes in B and R (M_B and M_R resp.). We used the $E(B-V)$ maps of Burstein & Heiles 1982 and derived the absorption coefficients using Savage & Mathis (1979) relations: $A_B = 4.0\ E(B-V)$ and $A_R = 2.52\ E(B-V)$.

3.4. $B-R$ color profiles

The method used to trace the $B-R$ color profiles is the same as in Paper I. We interpolated the surface brightness (SB) profiles in B and R because the sampling of the profiles are different in each band, and subtracted the resulting profiles from one another. The results are in excellent agreement with those obtained directly by performing the photometry on $B-R$ two-dimensional maps of several galaxies (Mk 996, Haro 14 and Fairall 301), only of better signal-to-noise toward the faint regions. Since we did not correct neither the profiles, nor the images from the seeing effects, the profiles are not to be seriously considered within the central first $1''$ radius.

The errors are calculated assuming that the errors in B and R are independent, using:

$$\sigma_{B-R} = \sqrt{\sigma_B^2 + \sigma_R^2}. \quad (5)$$

Here, we should emphasize that, in the central part of the BCDGs, the $B-R$ colors could be contaminated by nebular emission such as H_α present in the R band filter. The equivalent width of this line reaches generaly a few hundreds of Angström, therefore it can contribute significantly within the R filter to the total R emission. The outer parts of the BCDGs, however, do not suffer from such contamination, since the emission can be supposedly attributed to the stellar component only.

3.5. Comments on individual objects

Most of our objects show several star forming regions or knots with $B-R$ colors different from those of their host galaxies. We note that the knots get bluer away from the photometric center of the galaxy. This behaviour could reflect a variation of internal reddening due to dust, or more likely an age spread. However, those objects do not show obvious presence of dust as the ratio between the recombination lines of hydrogen Hα/Hβ remains close to a value of 3. Some galaxies have a single compact star forming knot ($\leq 5-10''$), whereas , in other galaxies, "multi-knots" regions are distributed over more than 2/3 of the galaxy's surface.

As in Paper I, the morphology of several BCDGs in the present sample departs conspicuously from axisymmetric shapes, for instance Tol 1937−423, UM 461, in the present sample. Because irregular morphology in star forming galaxies can be explained by mergers and dynamical interaction, and because our galaxies are not associated with known companions (except UM 465), we have searched for faint galaxy companions close to our BCDGs on our deep optical images. The results are presented in Sect. 4.3. We discuss now in detail the properties of individual galaxies. Other distortions (boxy isophotes, isophote apparent major axis rotation) are noted in the inner regions of several galaxies.

A summary of the anomalies noted in the BCDGs studied in our sample is given in Table 4 at the end of this section.

- **Haro 14** (NGC 244, VV728; North up, East left): this galaxy has several blue knots ($0.5 \leq B-R \leq 0.8$) embedded in a bright amorphous central region out of which several curved chain-like features are protruding. These "chains" have a knotty structure and are perhaps chains of star clusters and their associated H II regions. The bright amorphous central region is off-centered with respect to the outermost isophotes of the galaxy. A redder, bright knot ($B = 18.19$, $B-R = 1.2$) seems to be a "nucleus" or a site of stellar formation more evolved than the bluest knots. These features are surrounded by a red, almost circular envelope containing also low brightness knotty structures. The surface brightness distribution in B and R shows two "plateau" components (less suggestive in B) at $r = 3.5''$ and $22''$, with a strong rise in luminosity towards the center due to the presence of the "nucleus". The overall shape remains close to an exponential distribution, implying that Haro 14 could be a disk–dominated object with a large amount of Population I objects. Those results are in very good agreement with those of Marlowe et al. (1997), at least up to $r_e = 25$ arcsec, which is their limiting radius.
  The integrated color of the galaxy is not very blue: $B-R = 1.1$, suggesting the presence of an evolved underlying stellar population, also indicated by the off-centered circular envelope.
- **Mk 996** (North up, East left): Previous observations of this galaxy made under poor atmospheric conditions, have been reported in Paper I. The new data

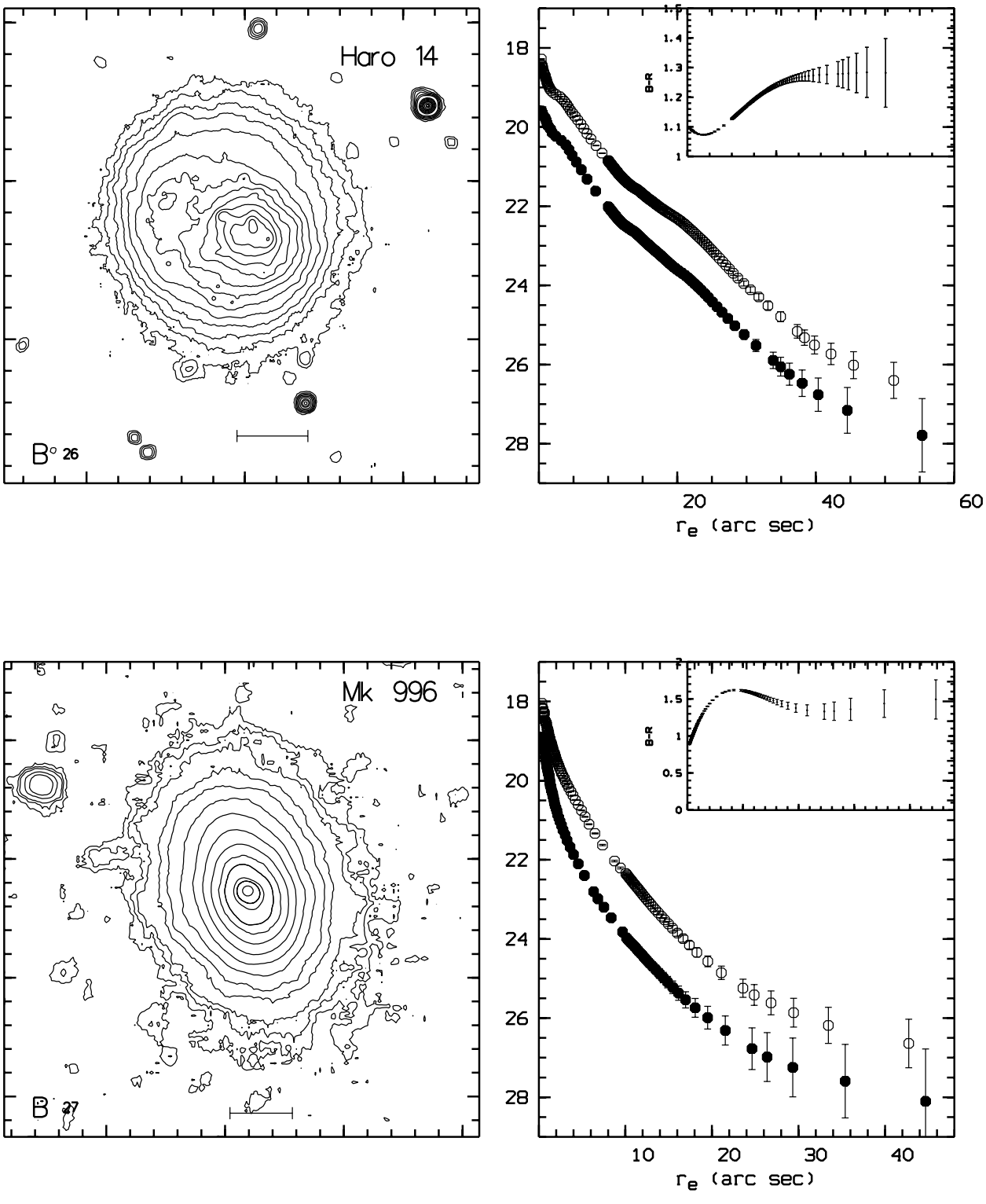

Fig. 1. **a)** Atlas of isophotal maps and surface brightness profile distributions. This atlas presents the isophotal B maps and surface brightness distribution in the B and R bands. On the top right corner, the $B-R$ color distribution is shown. The scale bar at the bottom of the map represents 1 kpc. The threshold brightness is indicated, the isophotal step on the map is 0.5 magnitude. Orientation is North up East left for the galaxies taken in December 1995, and North down and East right for the images taken in April-May 1995

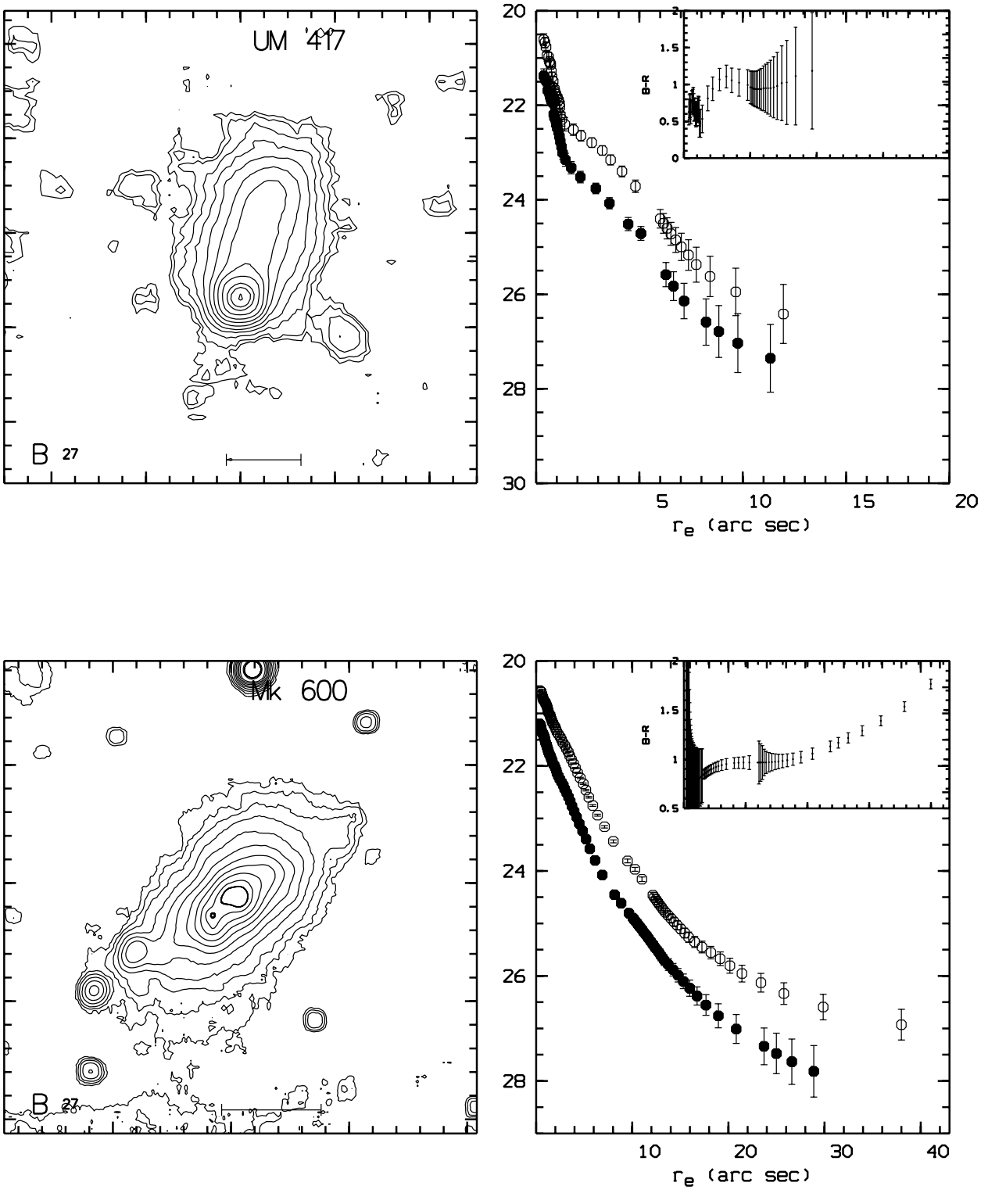

Fig. 1. b) continued

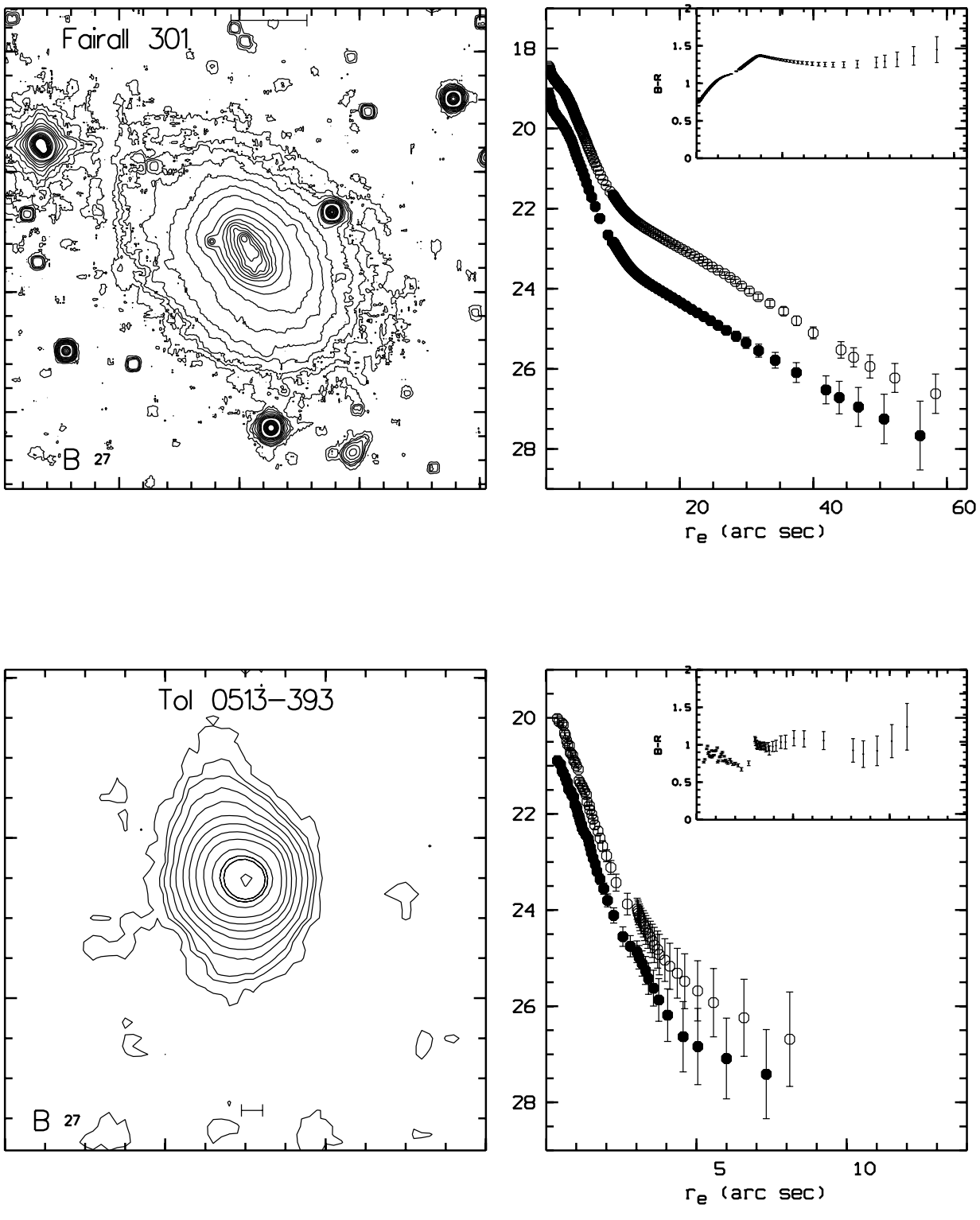

Fig. 1. c) continued

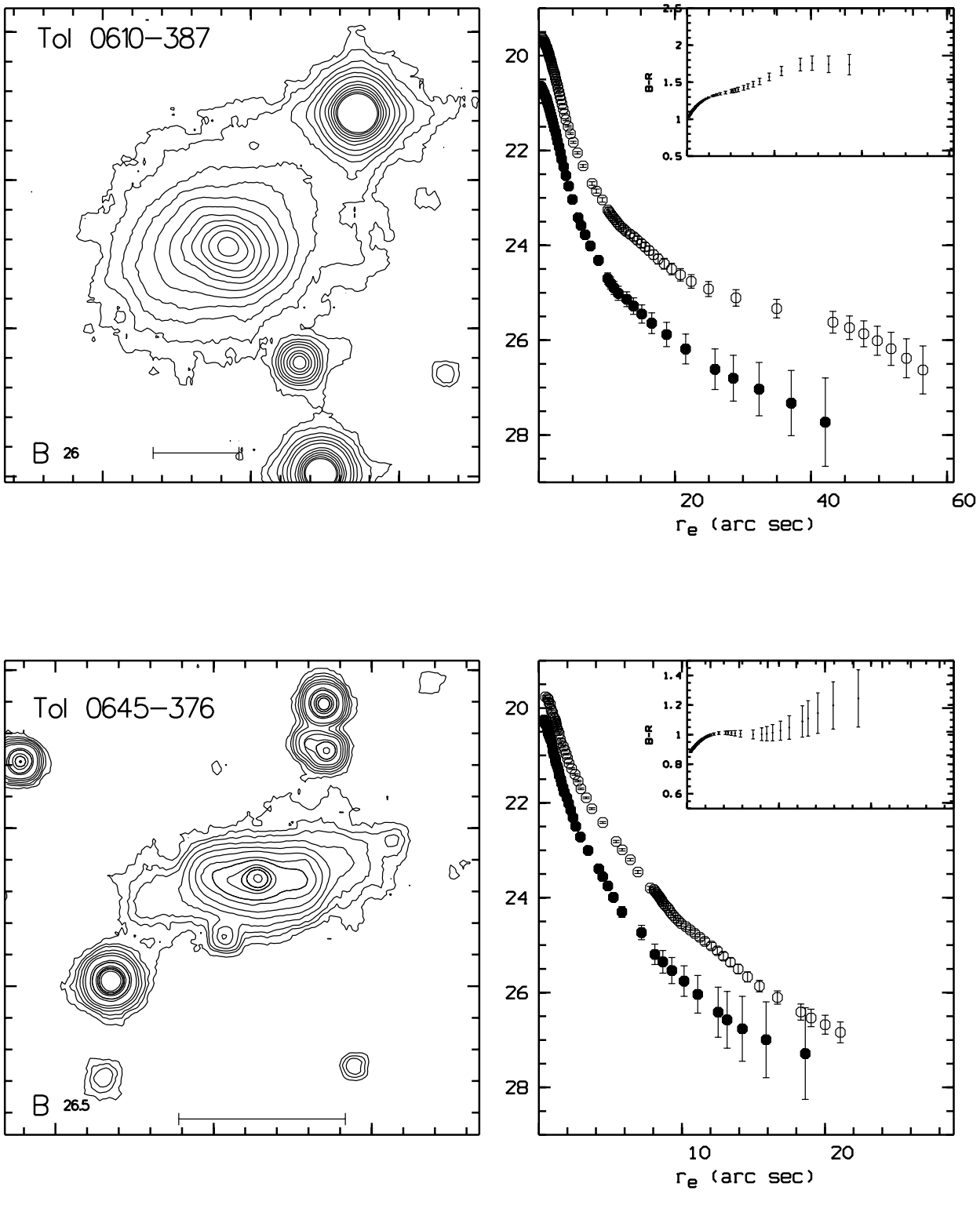

Fig. 1. d) continued

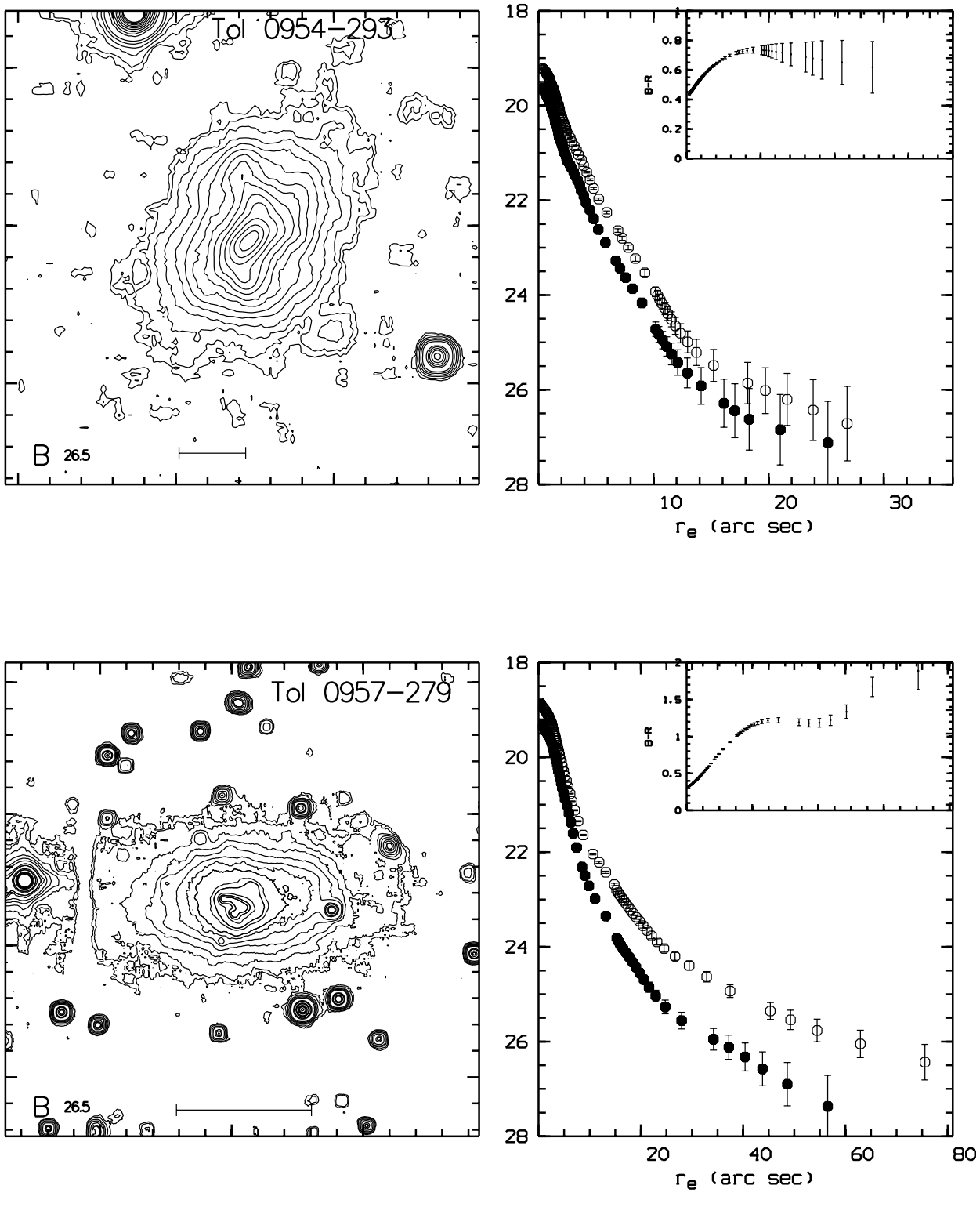

Fig. 1. e) continued

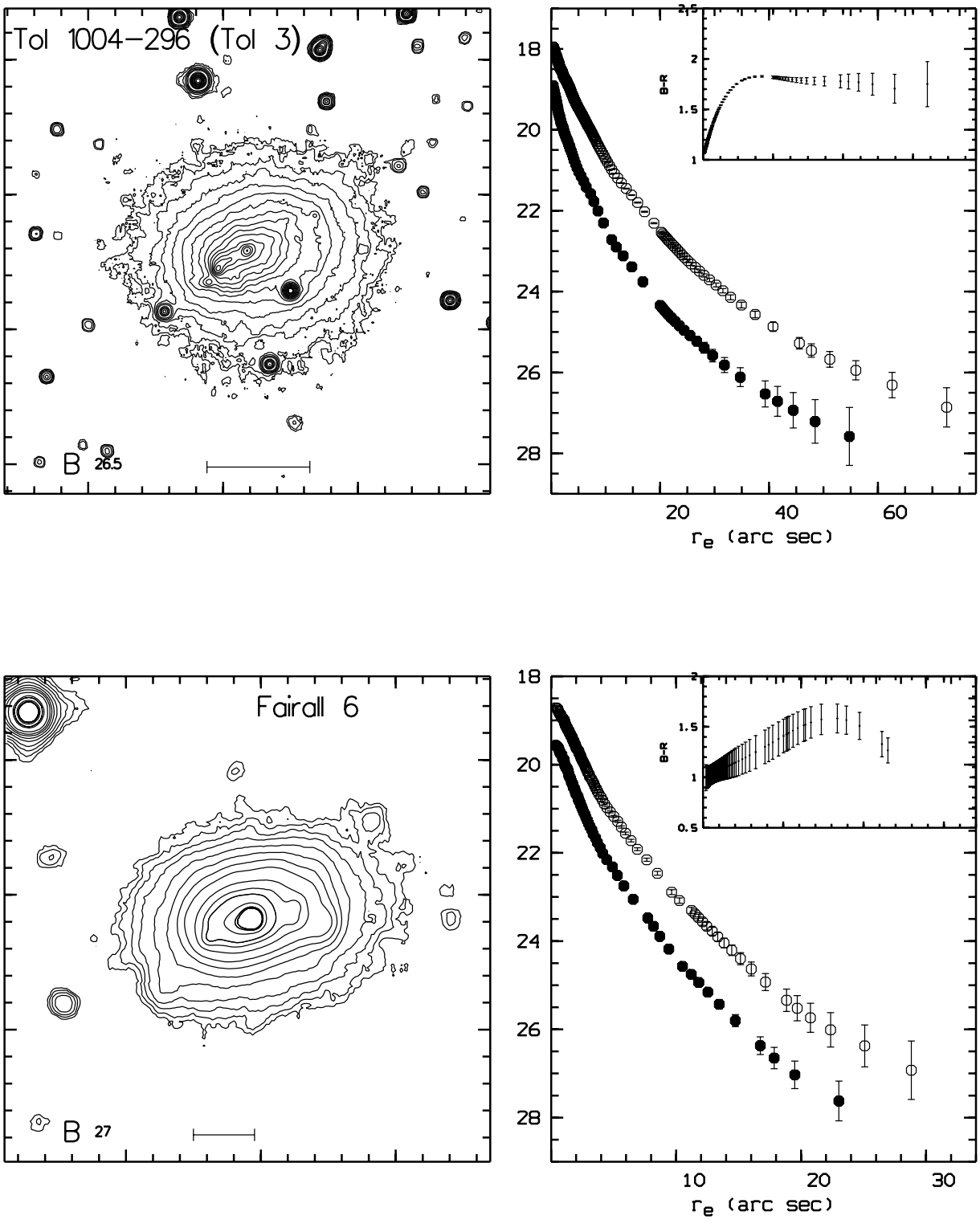

Fig. 1. f) continued

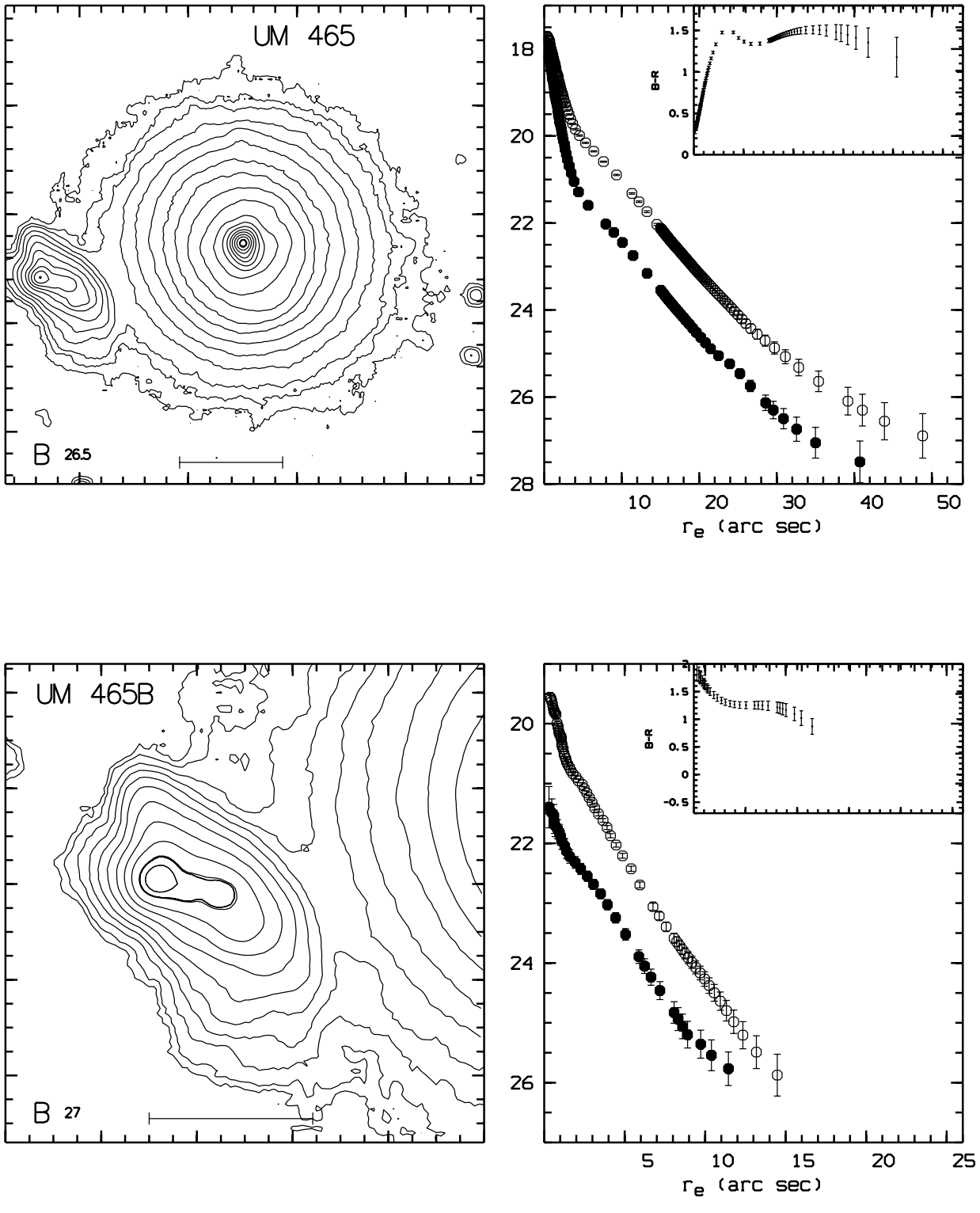

Fig. 1. g) continued

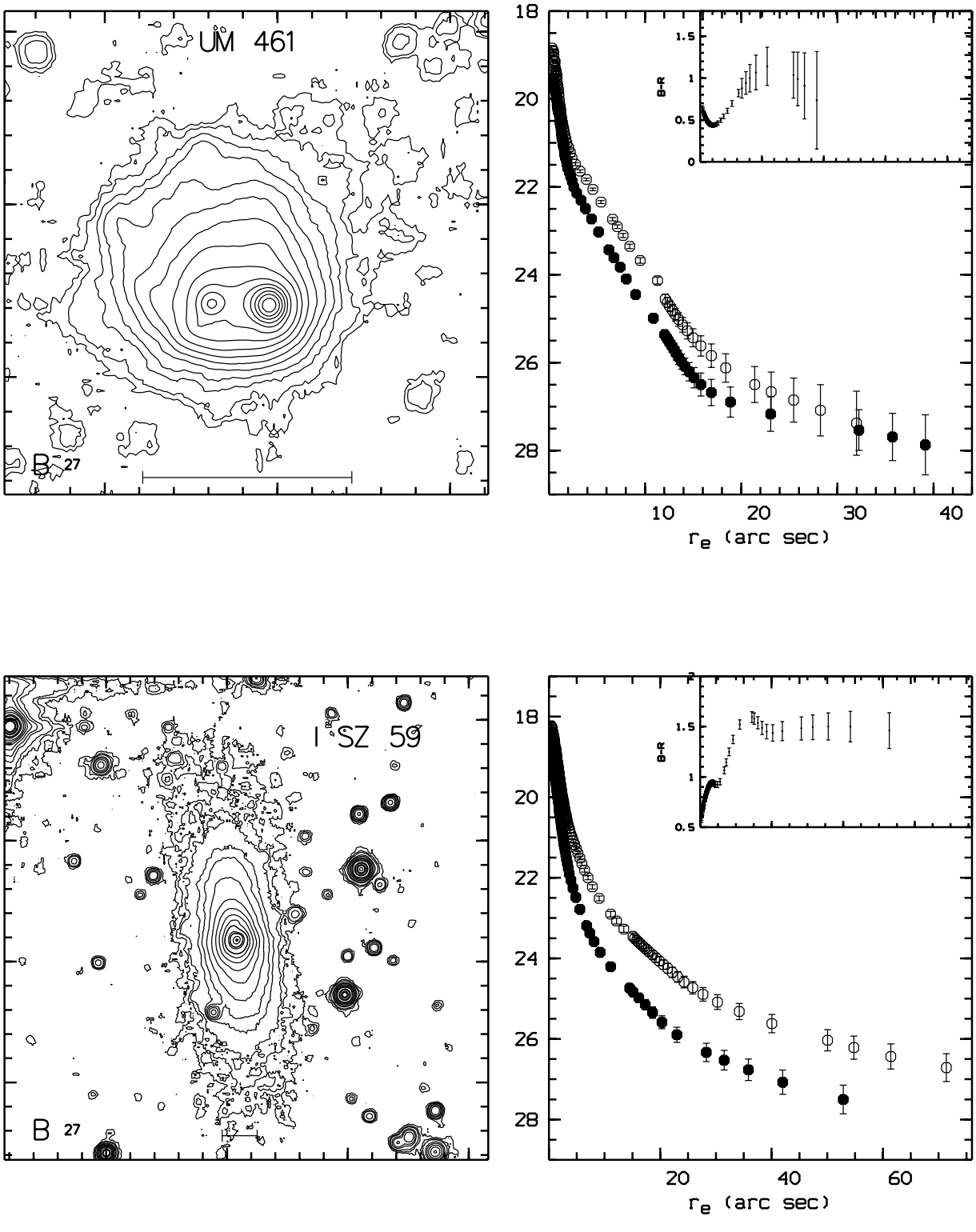

Fig. 1. h) continued

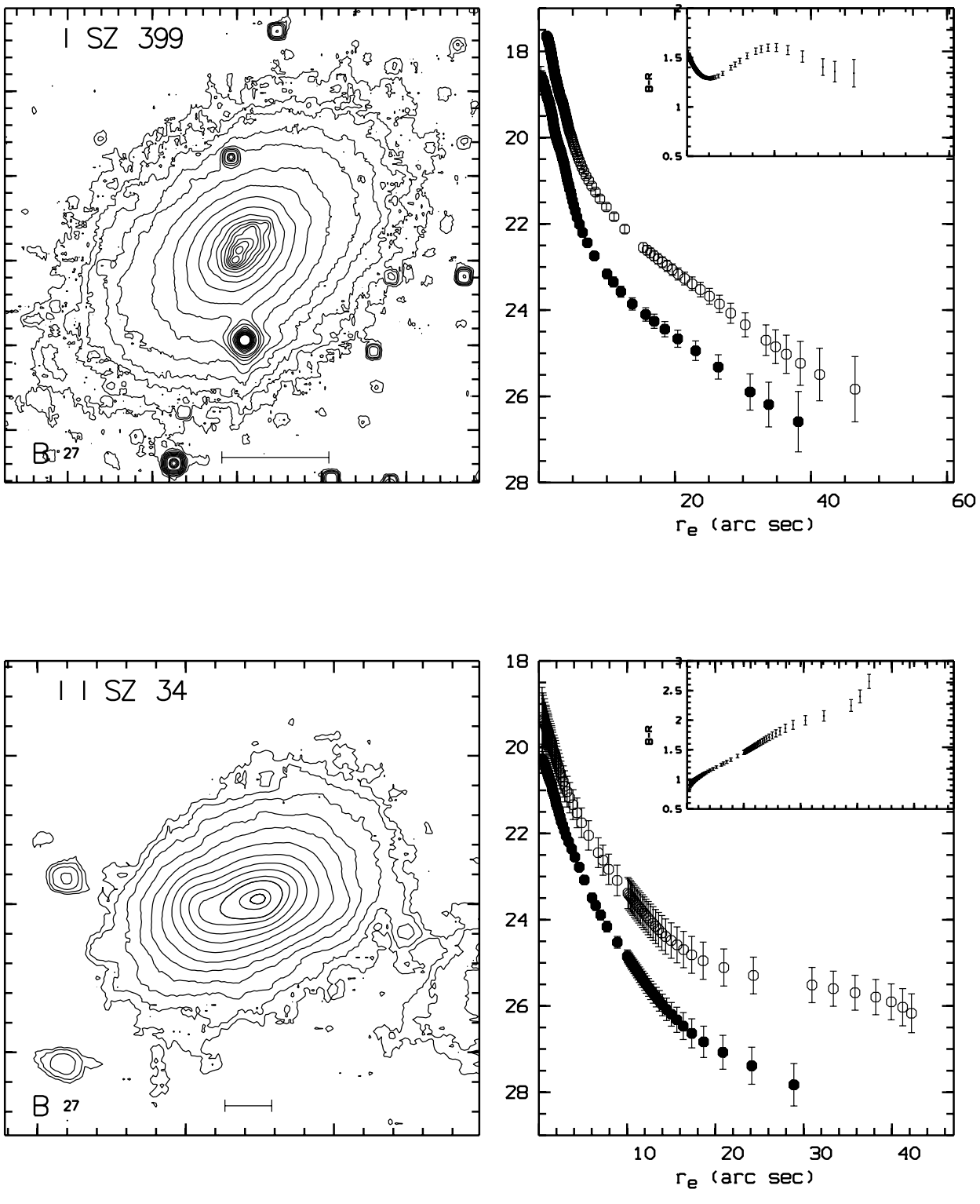

Fig. 1. i) continued

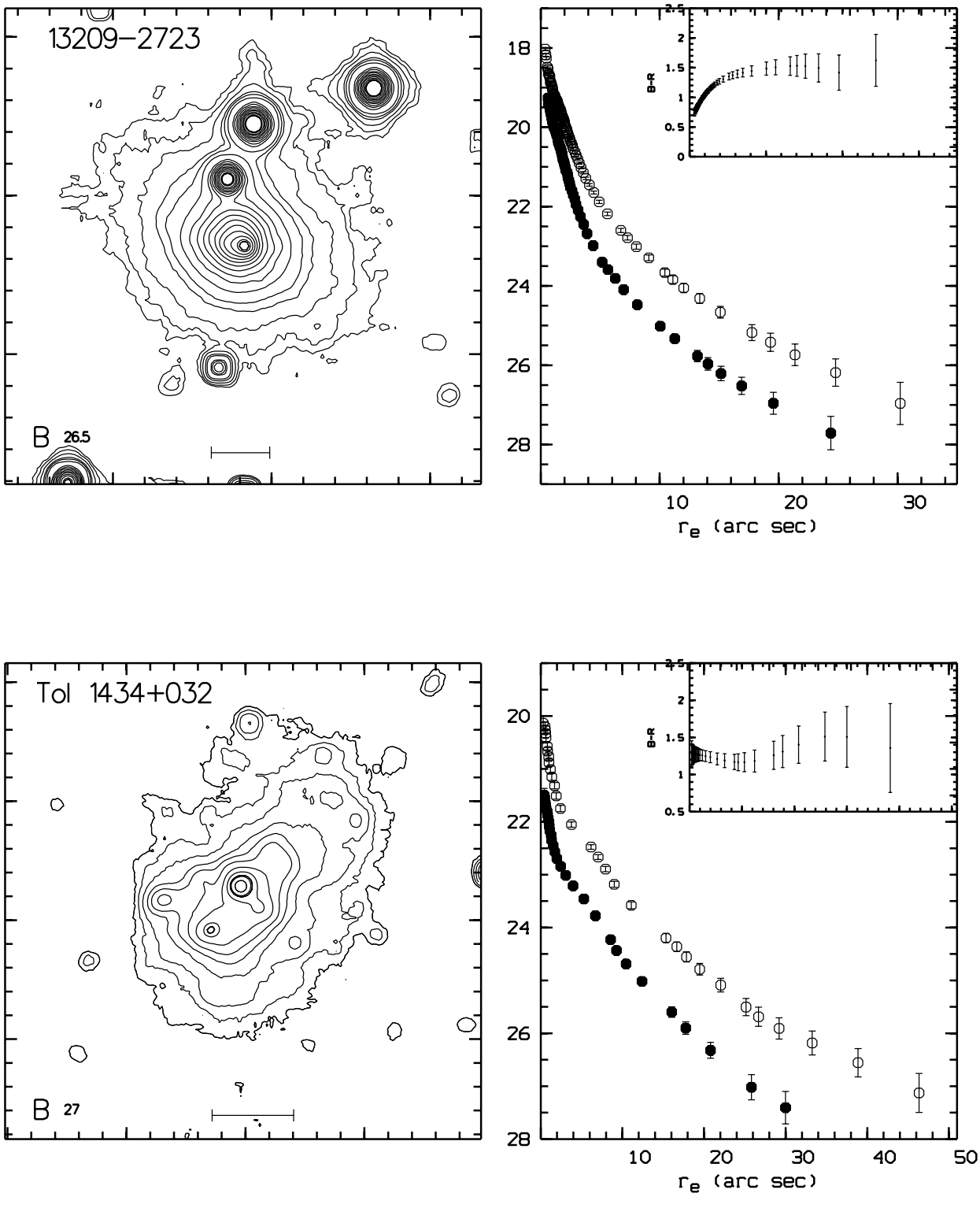

Fig. 1. j) continued

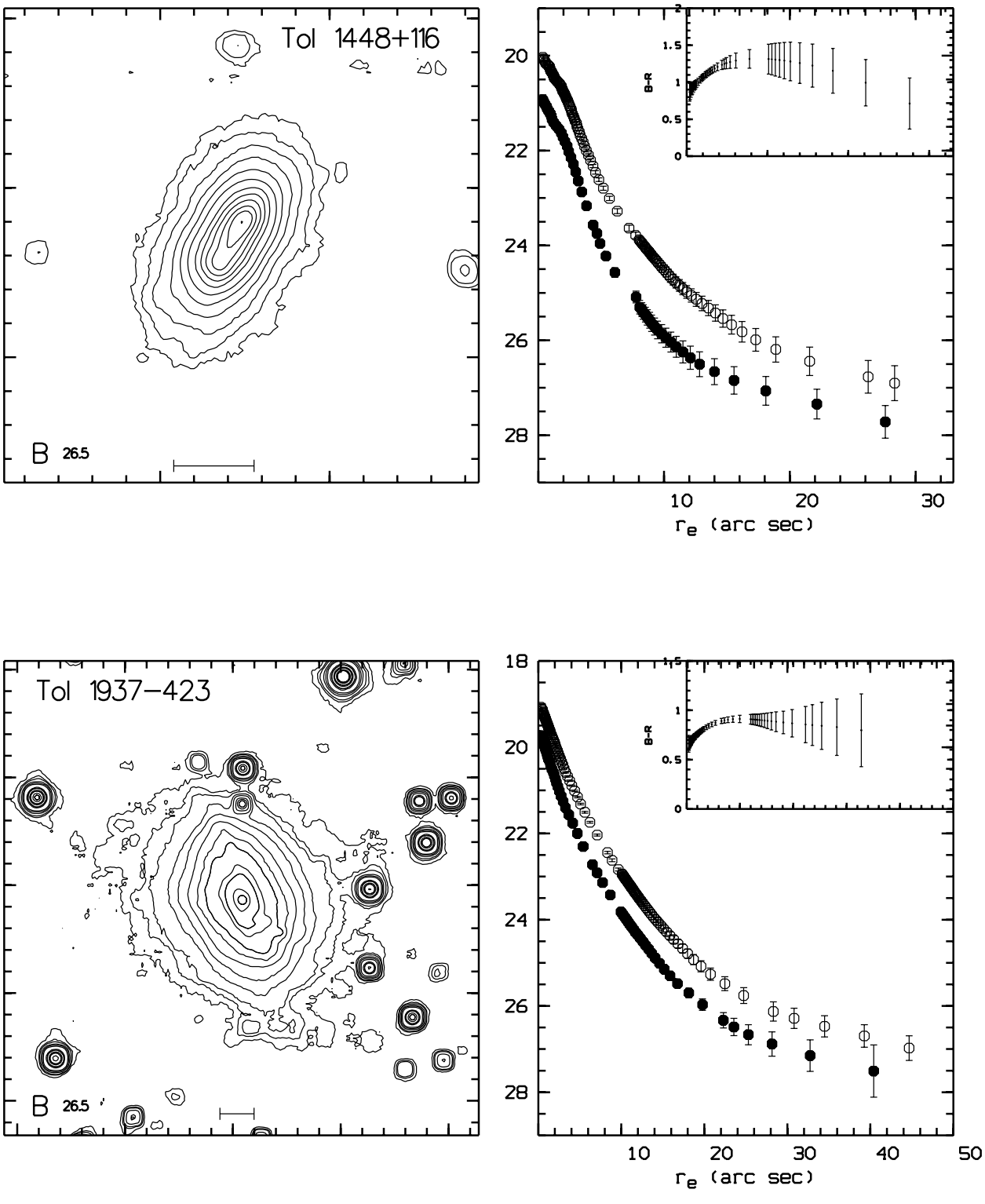

Fig. 1. k) continued

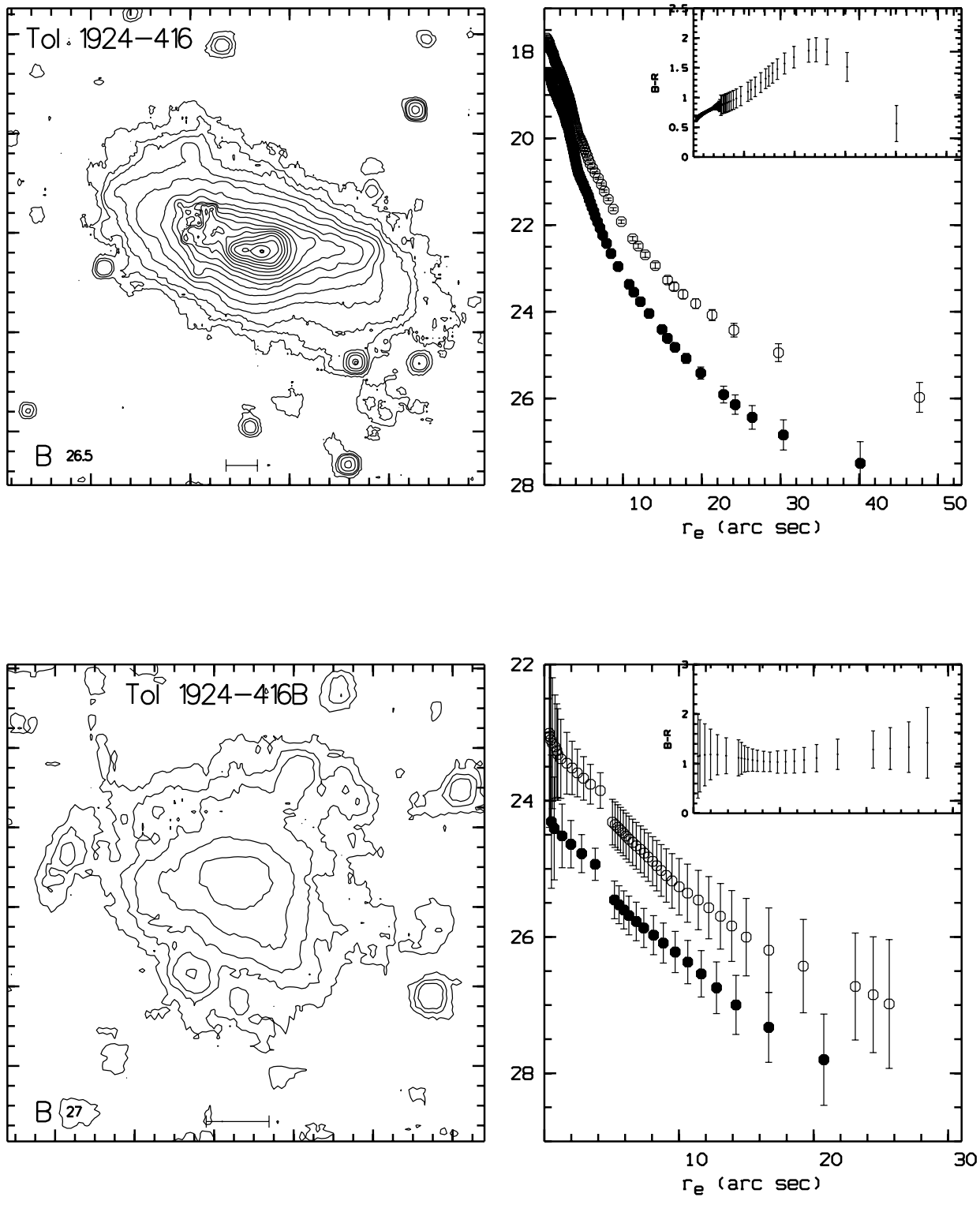

Fig. 1. l) continued

Table 3. Results of the photometry

Object [B]	m_B(asympt)	$\mu_{\rm eff}(B)$[mag/arcsec^2]	$<\mu_{\rm eff}>[B]$	$r_{\rm eff}(B)[''] $	$r_{0.25}(B)[''] $	r_{26}(B)[$''$]	$C_{21}(B)$
$''$ [R]	$B-R$ (asympt)	$\mu_{\rm eff}(R)$[mag/arcsec^2]	$<\mu_{\rm eff}>[R]$	$r_{\rm eff}(R)[''] $	$r_{0.25}(R)[''] $	r_{26}(R)[$''$]	$C_{21}(R)$
Haro 14	13.92	22.47	20.58	12.18	5.96	35.76	2.04
	1.11	21.26	19.46	12.10	5.90	43.96	2.05
Mk 996	15.35	23.12	20.89	7.23	2.82	23.71	2.56
	1.36	21.83	19.75	8.02	3.39	31.44	2.37
UM 417	18.13	24.74	23.29	5.18	2.49	6.94	2.08
	0.78	23.77	22.80	4.94	2.48	10.0	2.00
Mk 600	15.47	23.23	21.16	7.74	3.47	15.04	2.23
	1.26	22.52	21.18	13.97	4.82	26.53	2.89
Fairall 301	14.15	23.05	20.51	10.54	4.17	39.40	2.53
	1.01	21.91	19.59	11.05	4.51	50.34	2.45
Tol 0513−393	18.67	23.71	22.12	1.96	0.85	3.88	2.29
	0.85	22.85	21.26	1.96	0.85	5.75	2.29
Tol 0610−387	16.02	24.51	22.33	10.32	3.50	20.62	2.95
	1.73	24.15	22.25	22.00	6.64	48.76	3.31
Tol 0645−376	16.84	24.27	21.88	5.76	2.06	12.14	2.79
	0.93	22.95	20.75	5.25	2.17	16.94	2.42
Tol 0954−293	15.76	22.49	20.50	5.01	2.37	17.11	2.11
	0.46	21.58	19.77	4.42	2.15	18.95	2.05
Tol 0957−279	14.08	22.28	19.89	8.23	3.73	35.75	2.21
	1.04	23.75	21.51	27.97	6.74	58.70	4.15
Tol 3	14.18	22.18	20.24	9.18	4.19	35.34	2.19
	1.49	20.60	18.77	9.28	4.84	59.27	1.92
Fairall 6	15.83	22.13	20.22	4.27	2.05	15.74	2.08
	0.84	20.77	18.79	4.19	1.85	21.56	2.26
UM 461	16.18	23.31	21.28	5.91	2.24	13.97	2.63
	0.73	22.89	20.97	7.17	2.99	18.87	2.39
UM 465	14.37	21.88	19.89	7.14	2.31	30.80	3.09
	1.21	20.97	19.28	9.44	4.30	38.13	2.19
UM 465b	16.77	24.83	22.72	8.75	3.86	17.29	2.26
	1.30	23.64	21.28	8.20	3.34	16.63	2.45
I SZ 59	15.27	23.85	21.18	8.57	2.68	28.37	3.20
	1.30	23.58	21.22	15.90	4.82	45.05	3.30
I SZ 399	14.50	21.97	19.60	5.88	2.37	32.43	2.48
	1.38	20.80	18.48	6.64	2.62	51.28	2.54
II SZ 34	16.28	23.24	21.23	5.52	2.44	14.24	2.26
	1.61	24.06	21.78	14.98	4.44	40.57	3.37
13209−2723	16.08	22.74	20.28	3.90	1.47	14.61	2.65
	1.25	22.29	19.87	5.75	2.19	25.24	2.62
Tol 1434+032	16.43	25.06	23.15	12.46	5.93	19.28	2.10
	1.43	24.30	22.44	17.39	7.24	33.89	2.40
Tol 1448+116	16.83	24.73	22.18	6.65	2.41	10.34	2.76
	1.14	23.69	21.29	7.44	2.74	19.26	2.71
Tol 1924−416	14.42	20.91	18.91	4.46	1.97	23.51	2.27
	0.90	20.26	18.27	5.04	2.65	23.83	1.90
Tol 1924−416b	17.77	25.99	24.69	13.70	8.01	11.24	1.71
	1.34	24.84	23.56	15.06	9.01	15.42	1.67
Tol 1937−423	15.43	22.88	20.88	6.94	3.18	21.04	2.18
	0.84	22.07	20.08	7.06	3.43	28.05	2.06

Column 1: Galaxy name.
Column 2: Asymptotic apparent B magnitude and asymptotic $B-R$ color.
Column 3: Surface brightness inside the effective radius in mag arcsec^{-2}.
Column 4: Mean effective surface brightness, in mag arcsec^{-2}.
Column 5: Equivalent effective radius, in arcsec.
Column 6: Equivalent radius encircling 1/4 of the total luminosity, in arcsec.
Column 7: Isophotal equivalent radius at $\mu = 26$ mag arcsec^{-2}, in arcsec.
Column 8: concentration index in B and R colors, defined as the $r_{\rm eff}/r_{0.25}$ ratio.

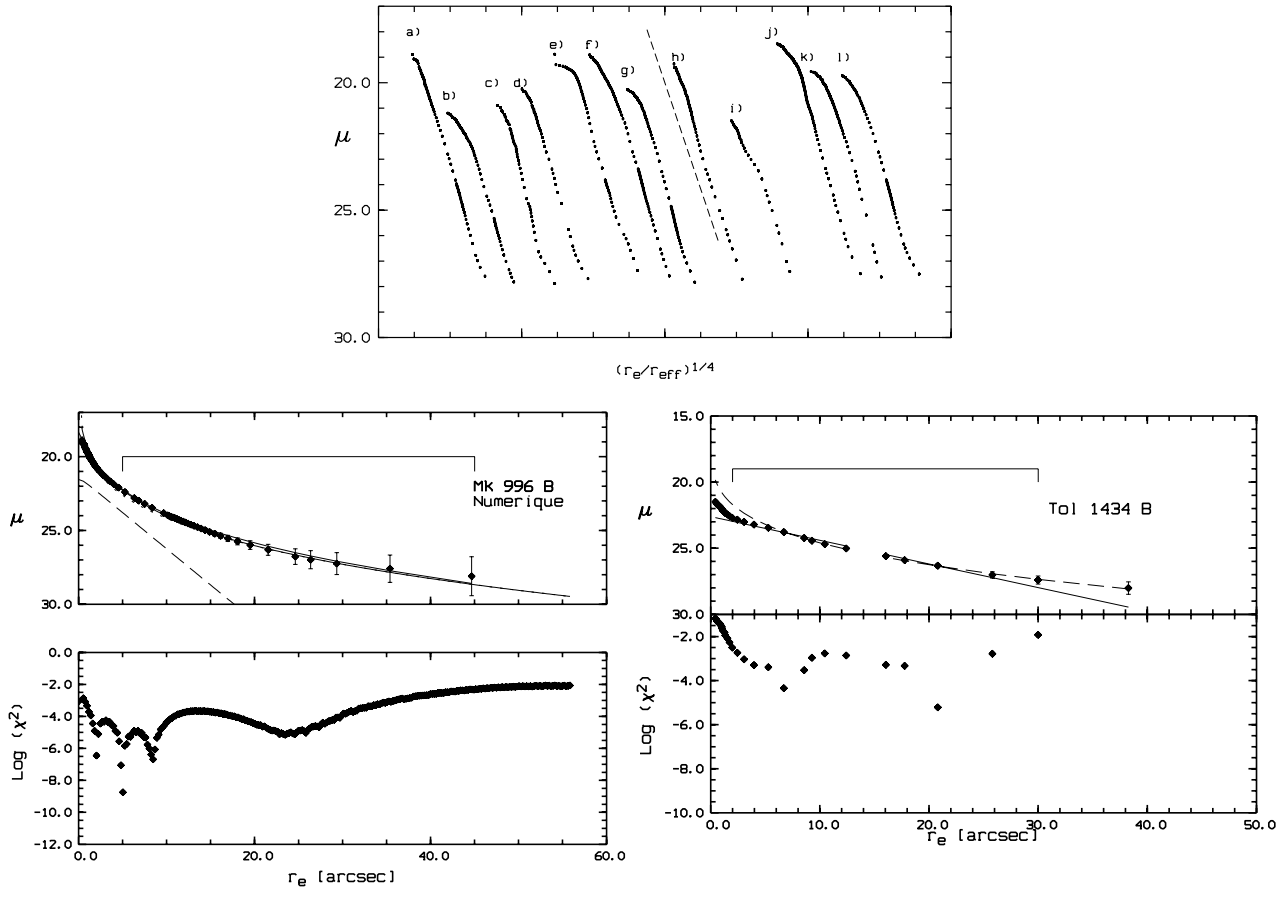

Fig. 2. **a)** B surface brightness distributions of the Elliptical-like BCDGs. The figure shows the B surface brightness distribution of the 13 objects whose SB distribution is clearly dominated by a $r^{1/4}$ law, as a function of the reduced variable: $(r/r_e)^{1/4}$, from the De Vaucouleurs law. The dashed line represents the slope of de Vaucouleurs law (8.327). **a)** Mk 996, **b)** Mk 600, **c)** Tol0513−393, **d)** Tol 0645−376, **e)** Tol 0957−279, **f)** Tol 1004−296, **g)** II SZ 34, **h)** 13209−2723, **i)** Tol 1434+032, **j)** Tol 1924−416, **k)** Fairall 6, **l)** Tol 1937−423 **b)** Profile decomposition of Mk 996: The figure shows the decomposition of the surface brightness profile of Mk 996 in the B band: the bold dashed line represents the exponential component, while the faint dashed line represents both the $r^{1/4}$ and exponential components. Note the presence of the compact exponential component in the central regions, it may be the exponential seen by Thuan et al. (1996) on their HST images. **c)** Profile decomposition of Tol 1434+032: the bold dashed line represents the exponential component, while the faint dashed line represents both the $r^{1/4}$ and exponential components. Note that the fit gives an excess of light in the central parts of the galaxy. It is probable that this galaxy possesses a core component much older that the star forming regions, as indicated by its red color

Table 4. Morphological anomalies of the sample

Two nuclei	Envelope distortion (cometary galaxy)	Boxy internal isophotes	Boxy external isophotes	rotating isophotes
SBS 1533	SBS 0940	Mk 900	SBS 1006	SBS 1054
Mk 324	SBS 1413	Mk 1434	SBS 1147	Mk 900
Mk 1416	Mk 1131	Mk 1499	SBS 1428	
Mk 1426	Mk 1450		Mk 900	
Mk 1499	Mk 1480		Mk 1416	
			Mk 1434	
Fair 301	UM 417	Tol 0954	Mk 600	Tol 0610
Tol 3	Tol 0610	II SZ 34	Fair 6	I SZ 399
UM 461	Tol 0645		I SZ 59	Tol 1434
I SZ 399	Tol 0954		II SZ 34	Tol 1924
	UM 461		Tol 1448	
	Tol 1924		Tol 1937	

establish the elliptical–like character of this object. This BCDG has a regular structure with slightly distorted isophotes near the center, due to the presence of a dust lane. The surface brightness distribution is largely dominated by a $r^{1/4}$ law, with one noted deviation: an excess of light between 5″ and 15″ (surface brightness of 22 mag arcsec^{-2} and 25 mag arcsec^{-2} repectively, see Fig. 2b). These present observations resolve the inconsistency between our results from Paper I and the high spatial resolution HST observations (WF-camera) of Thuan et al. (1996). They have performed surface photometry of this galaxy, and fitted their observations with an exponential up to a radius of 20″, and reported the presence of an excess of light at larger radii. Indeed, our data which are deeper and show a larger part of the galaxy, definitely show this

excess. The surface brightness distribution is better fitted by a $r^{1/4}$ law with a small compact exponential component in the central regions.

- **UM 417** (North up, East left): this cometary-like faint BCDG has a bright compact star forming region at the South-East end. The light distribution is well fitted by neither a pure exponential nor a $r^{1/4}$ law. The profile shape is very similar to that of SBS 1331+493, a galaxy from our Northern Sample (Paper I). The color distribution wriggles near the center with a zero colour gradient, the center being bluer.
- **Mk 600** (North up, East left): Kinman & Davidson 1981Kinman & Davidson (1981) give a photographic B magnitude inside the Holmberg diameter of 15.42, in excellent agreement with our measurement, $B = 15.47$. This galaxy has a blue core ($B - R \sim 0.5$) embedded in a diffuse bright area elongated along the major axis. Another small star forming region ($B - R \sim 0.4$) is conspicuous at $13''$ South-east of the center. The outer/low surface brightness envelope has a boxy shape with a redder color $B - R \sim 1.5$ with a strong center-to-edge color gradient. Two small angular diameter objects are located to the South-East of the isophotes of Mk 600. The closest has a diameter of $13''$, and is elongated along the major axis of the main galaxy with a North-West extension. The second object is also resolved ($FWHM$ of $2.5''$), located further away along the major axis. Without spectroscopic redshift, the nature of these objects is uncertain. Nevertheless, their magnitudes 18.90 and 20.50 (B and R respectively), and their colors $B - R \sim 0.6$ and 1.1, suggest the possibility that they are faint galaxy companions near Mk 600. At the North-West boundary of Mk 600, a low surface brightness blue extension is also detected. The surface brightness distribution of Mk 600 is consistent with a dominant $r^{1/4}$ law, but some deviations are obvious.
- **Fairall 301** (NGC 1522; North up, East left): the RC3 catalog (De Vaucouleurs et al. 1991) quotes a total B magnitude of 13.93 ± 0.13 from Bergvall & Olofsson 1986, comparable to our measured B of 14.15 mag.
  This BCDG is embedded in a faint envelope; it has regular isophotes, a bright blue core ($B - R \sim 0.5$), with two separated knots slightly off-centered. The brightness gradient towards the outer regions is more pronounced on one side (North-East) than the other. The major axis of the central star-forming region does not coincide with that of the whole galaxy. The SB distribution beyond a radius of $10''$ is dominated by an exponential law.
- **Tololo 0513−393** (North up, East left): this is a very compact blue galaxy, barely a dwarf with $M_B = -17.66$, showing faint North-South extensions. The nucleus is off-centered with respect to the outer isophotes. The surface brightness distribution is consistent with a dominating bulge-like structure and a faint underlying exponential component. The morphology is difficult to ascertain because of the small angular size ($r_{26} \sim 4''$) due to the large distance of this galaxy, the most distant in our sample with a recession velocity of 14370 km s^{-1}. The color distribution shows no large color gradient; but the outer parts are redder than the central parts. There is some evidence for blueing at $r_e = 3''$ in our data, and Terlevich et al. (1991) report a Balmer decrement of 3.45 in the central star forming region. Thus, the red color of the nucleus is most probably due to dust extinction inside the starforming region, rather than caused by an evolved star population.
- **Tololo 0610−387** (North up, East left): this slightly distorted galaxy shows a small blue South-West extension ($B - R \sim 0.8$). The isophotes appear to be rotating, although the presence of foreground galactic stars may alter the shape of the outer isophotes. The surface brightness distribution is slightly different in B and R. It is well fitted by an exponential in the B band, but in the R band, a two component profile is required: an exponential that follows the B surface brightness distribution, and a shallower redder envelope. This galaxy is red in our sample ($B - R = 1.76$); it has a strong gradient in $B - R$, the center being much bluer: $B - R \sim 0.9$.
- **Tololo 0645−376** (North up, East left): This intrinsically luminous object ($M_b = -17.97$) is not a dwarf galaxy by our selection criteria (absolute magnitude fainter than −16.5). it is blue ($B - R = 0.97$), large ($r_{26}(B) \sim 5$ kpc), and elongated along the East-West direction. It displays a central star forming region distributed along the major axis, with a bright stellar-like nucleus ($FWHM = 1.6''$). The outer envelope shows two weak extensions, reminiscent of warps present in the outer parts of some edge-on disk galaxies, but these features, also visible on the $B - R$ map could be tidal remnants from a past interaction. The $B - R$ map shows a local maximum West of the center, extending North-West, that suggests the presence of a dust lane obscuring partly the star forming region. The Balmer decrement value, Hα/H$\beta \sim 4.3$, observed by Terlevich et al. (1991) supports the hypothesis of some dust content. On the isophotal map, the extension visible South-East from the center is caused by a superimposed faint blue Galactic star. The surface brightness distribution is consistent with a dominant $r^{1/4}$ law with a moderate color gradient.
- **Tololo 0954−293** (North up, East left): the only available other photometric measurement is from Bohuski et al. (1978), who gives $B = 16.61$ inside an aperture of $11.6''$, which compares to our measurement of $B = 16.49$.
  The recession velocity of this galaxy is 2055 km s^{-1}; it was kindly supplied to us by G. Dudziak (private communication), inferring $M_B = -16.26$.

The morphological structure of this galaxy is reminiscent of the Magellanic type galaxy NGC 4449, or II ZW 33 (Loose & Thuan 1986b). A very blue ($B-R$ $\sim$ 0.4), extended, bar-shaped star forming region out of which protrude two opposite clumpy extensions, is embedded in a boxy envelope. The surface brightness profile is composite: the inner regions can be fitted by an exponential law with a steep central braightness gradient; and a very shallow outer envelope can be fitted by another exponential law with a faint central brightness.

- **Tololo 0957−279** (Tololo 2; North up, East left): the galaxy has an amorphous overall shape; it is elongated along an East-West direction. The bright central region shows a complex pattern, with a curved chain of luminous blue knots ($B-R \sim 0.3$). The brightest knot near the center is elongated like the "mini-bar" seen in numerous hot-spot galaxies (dwarf HII hotspot galaxies, Salzer et al. 1989b) The $B-R$ color contours suggest the presence of a dust lane across the star forming region. A large, red and shallow extension around the bright central region is visible along the major axis. The B and R band surface brightness distributions are both consistent with a dominant $r^{1/4}$ law with some local deviations. In addition, the envelope beyond $r = 25''$ indicates the presence of an underlying exponential component. This is in agreement with Kunth et al. (1988) observation that the disk component accounts for only one third of the luminosity of Tololo 2. We also note a strong color gradient in the outer regions, where the outermost parts of the envelope become very red.
- **Tololo 1004−296** (Tololo 3, NGC 3125; North up, East left): for this BCDG, we obtain a total B magnitude of 14.2 which is 0.7 magnitude fainter than Bergvall & Olofsson (1986) value, quoted in RC3, and 0.1 brighter than Kunth et al. (1988)'s value. The presence of 3 superimposed Galactic stars falling within the aperture used by Bergvall & Olofsson could explain the measurement discrepancies.
  The overall shape is roughly elliptical with an elongated bright central region of asymmetric brightness distribution. An elongated bright knot pointing North-East of the central "nucleus" leads to a morphology similar to that of Fairall 301. The bluest knot in the star forming region has a $B-R$ color of 1.1, suggesting the presence of an evolved stellar population. The surface brightness distribution is consistent with a dominant $r^{1/4}$ law, in agreement with another photometric observation of this galaxy (Kunth et al. 1988).
- **Tololo 1108+098** (Fairall 6; North is down, East right): This object shows a kidney–like bright central region with a compact blue ($B-R \sim 0.2$) nucleus ($FWHM = 2''$). Several connected knots are grouped along a curve extending East-West from the center. These features are star-forming sites, as evidenced by their blue colors ($B-R \sim 0.4$). The outer envelope is elliptical with a boxy shape. The surface brightness distribution is fairly consistent with a dominant $r^{1/4}$ law, although there is a break in the light profile at about $4''$ from the center coincident with the two secondary star forming regions.
- **UM 465A and B** (Mk 1308, IC 745; North down, East right): Data for this pair of galaxies previously observed by us at the Pic du Midi Observatory, were published in Paper I. The present La Silla data have a better S/N ratio. It allows us to derive the surface photometry of the companion, UM 465B which is separated from the main galaxy, UM 465A, by $38''$ (2 kpc projected distance). The main galaxy has regular external isophotes; they become asymmetric towards the center, and there is a steep surface brightness gradient opposite to the companion direction. The color maps show that the star formation event occurs in the center and produces a small extension in the North-East direction. High spatial resolution HST images (WFPC2, archive images) show clearly the extension due to a chain of star forming knots extending south. A dust lane is also clearly visible north of the center.
  The companion exhibits a high surface brightness knot and a tail extending opposite to the direction of the main galaxy. The bright compact knot of the companion is very red ($B-R \sim 1.8$) and may be the obscured nucleus. The star forming region extends across the whole companion ($0.5 \leq B-R \leq 0.9$), a possible consequence of the gravitational interaction between the two galaxies.
  Both galaxies have dominant exponential surface brightness profiles with very steep surface brightness gradients in B and R, but departures from the pure exponential law are obvious.
  Salzer et al. (1989b) give a total B magnitude of 14.14, and a $B-R$ color of 1.24 for UM 465A, in fair agreement with our values.
- **UM 461** (North down, East right): This small galaxy with a double nucleus exhibits an external envelope distorted strongly towards the South-West, suggesting a recent tidal event. This is strongly supported by the fact that UM 461 belongs to a small group of dwarf galaxies including UM 462. However, the recent HI observations done by Van Zee et al. (1998) tend to show that no tidal interaction takes place.
  The two "nuclei" do not have the same color: the brighter ($B = 17.41$) is bluer ($B-R \sim 0.5$) compared to the other with $B = 18.62$ and $B-R \sim 1.1$. The surface brightness distribution is composite and is fitted by the sum of two exponential laws. The outer envelope (beyond $B = 26.75$ mag/arcsec^2 and $R = 26$ mag/arcsec^2) has a very shallow brightness gradient. Moreover, the HI maps obtained by Van Zee et al. (1998) indicates a velocity gradient within the galaxy along the same axis defined by the two star forming

knots, while the nominal kinematic center more or less coincides with the reddest knot. The morphology of this object could suggest the merging of two dwarf galaxies before final relaxation or dynamical reconfiguration.
Salzer et al. (1989b) give a total B magnitude of 16.35 with $B-R=0.93$, in acceptable agreement with our values: $B=16.18$ and $B-R=0.73$.

- **I SZ 59** (North down, East right): Described as "spherical" by Rodgers et al. (1978), this object, in fact, is very elongated on our deep images, with regular elliptical outer isophotes. The central core has circular inner contours that become boxy at $r=6''$. There is no isophote rotation. From the $B-R$ color map, the starburst seems to be confined to the center of the galaxy. The surface brightness distribution is fitted with a $r^{1/4}$ law in the central region, whereas the light distribution in the envelope is fitted by an exponential with a shallow brightness gradient.
- **I SZ 399** (North down, East right): Described as "elliptical" by Rodgers et al. (1978), this galaxy exhibits a regular structure except in the bright central core where a double nucleus is present. The environment of this double nucleus shows irregular contours with isophotal rotation. The central star forming region extends ∼500 pc across along the South-West direction. The surface brightness distribution is well represented by an exponential law, except in the central region ($r \leq 7''$) where a steep brightness gradient, perhaps caused by a bulge, is present.
- **II SZ 34** (North down, East right): this is an elliptical–like galaxy, in the NGC 5073 group, which is also close on the sky to an edge-on galaxy (MCG 2-34-24) showing strong absorption lines. The isophotes are disturbed and boxy. The central part of the galaxy shows a curved shape, and our $B-R$ color map infers that the star forming region extends along the major axis. The surface brightness distribution is well fitted by a $r^{1/4}$ law, and a red envelope is seen from the $B-R$ color excess.
- **13209−2723** (North down, East right): This compact elliptical–like galaxy was discovered in the ESO Prism Objective Survey (Surace & Comte 1994). The galaxy shows a slightly off–centered star forming region. The surface brightness distribution is well fitted by a $r^{1/4}$ law in the B and R bands. The morphology is difficult to ascertain because of three foreground bright stars on top of the southern half of the galaxy.
- **Tololo 1434+032** (Fairall 42; North down, East right): this object looks like a Magellanic type galaxy with several star forming knots of red colors (from $B-R \sim 1.3$ to 1.9). The $B-R$ color map shows that the knots are connected to each other. The brightest knot is located at the center of the outer isophotes. At low surface brightness levels (26 mag/arcsec^2), the B and R images show a red regular elliptical envelope, the major axis of which does not correspond to the major axis of the star forming region. The surface brightness distribution is neither a pure $r^{1/4}$ nor exponential law. There is a steep surface brightness gradient towards the center corresponding to the position of the brightest knot. The photometric decomposition of the surface brightness profile reveals the presence of two distinct components: an exponential component with a steep surface brightness gradient, and a low surface brightness underlying component fitted by a $r^{1/4}$ law (see Fig. 2c).
Bohuski et al. (1978) give $B=17.69$ inside an aperture of 11.6″, in agreement with our measured B value of 18.10 mag in the same aperture.
- **Tololo 1448+116** (Fairall 44; North down, East right): it is another elliptical–like galaxy showing a star formation region distributed along the major axis. The brightest part of the galaxy has a reddish color of 0.9, and it is off-centered in the North-East direction. The isophotes are boxy without rotation. The surface brightness distribution is composite: a high surface brightness component, possibly a bulge, follows an $r^{1/4}$ law, and a faint surface brightness component, very shallow, is fitted by an exponential law. The color distribution shows a blueing of the external parts of the galaxy.
- **Tololo 1924−416** (North down, East right): this BCDG is compact ($r_{\rm eff}=752$ pc), luminous ($M_B=-18.29$) for a radius of $r_{26}=3960$ pc in B, and a color $B-R=0.90$. An IRAS source (Fehmers et al. 1994) has been detected at its position, indicating a significant amount of dust somewhere in the BCDG. However, the star formation region does not seem to contain much dust, according to a low Balmer decrement value H_α/H_β of 3.1 (Storchi-Bergmann et al. 1995). This galaxy shows many peculiar features: rotating disturbed isophotes, off-centered bright young star forming clusters. HST images (Meurer et al. 1995) shows that the central SF region is resolved in very young star clusters. The $B-R$ color map shows that the star formation occurs in the center of the galaxy, and that it is also spread along the major axis. The surface brightness distribution of the main galaxy is well fitted by a $r^{1/4}$ law for a surface brightness level fainter than 21 B mag/arcsec^2 (20.5 in R), whereas in the inner regions, the distribution is dominated by the central peak, that could be a bulge. Tololo 1924−416 has a very faint neighbour ($m_b=17.8$) separated by 142″ North-West from the BCDG (or 24 kpc, at the same distance). This galaxy looks like a Magellanic dwarf of low surface brightness with a $B-R$ color of 1.3 similar to that of the UM 465 companion. The external isophotes of Tololo 1924−416 extend towards the faint object. The surface brightness distribution of the candidate companion can be fitted by an exponential law with large uncertainties in the fit due to a lower signal-to-noise. At the time this

Table 5. Exponential galaxies: north and south samples

Object	$\alpha_0(B)$	$\alpha_0(R)$	$\mu_0(B)$	$\mu_0(R)$	Composite
Haro 14	2.54 ± 0.05	2.74 ± 0.04	20.63	19.10	
UM 417	0.79 ± 0.14	0.81 ± 0.04	26.55	25.78	
Fairall 301	2.56 ± 0.12	2.41 ± 0.05	22.23	21.00	
Tol 0610−387a	1.48 ± 0.01	1.44 ± 0.01	23.40	21.98	C
Tol 0610−387b	0.87 ± 0.01	0.45 ± 0.01	24.50	23.88	
Tol 0954−293a	4.09 ± 0.02	3.73 ± 0.01	19.79	19.35	C
Tol 0954−293b	0.63 ± 0.05	0.84 ± 0.03	25.13	23.94	
UM 461a	7.57 ± 0.17	7.81 ± 0.12	21.34	20.44	C
UM 461b	1.11 ± 0.09	2.30 ± 0.23	26.01	24.33	
UM 465A	3.70 ± 0.04	3.12 ± 0.06	20.39	19.46	
UM 465B	6.83 ± 0.02	7.62 ± 0.01	21.72	20.10	
I SZ 59a	1.56 ± 0.03	1.42 ± 0.03	22.64	21.44	C
I SZ 59b	0.48 ± 0.03	0.40 ± 0.04	25.17	24.08	
I SZ 399	2.75 ± 0.17	2.73 ± 0.07	22.20	20.83	
Tol 1448+116	0.73 ± 0.06	–	25.50	–	C
Tol 1924−416B	0.87 ± 0.03	0.94 ± 0.04	24.76	23.59	
SBS 0940+544c	1.11 ± 0.05	1.12 ± 0.07	22.39	21.78	
SBS 1006+578	0.51 ± 0.04	0.40 ± 0.02	20.64	20.07	C
SBS 1428+457	0.98 ± 0.03	1.03 ± 0.03	20.37	18.90	
SBS 1533+574	– –	0.97 ± 0.02	–	18.38	?
Mk 1416	1.04 ± 0.05	1.19 ± 0.02	20.61	20.11	
Mk 1423	–	0.65 ± 0.04	–	15.06	C
Mk 1481	2.42 ± 0.06	1.87 ± 0.08	21.64	23.41	

Scalelength in B and R are given kpc^{-1}.

article was written, the nature of this neighbour was not known; since then, its recession velocity was measured by Östlin et al. (1998) confirming that it is indeed a companion of Tololo 1924−416.
In the contour plot of Tololo 1924−416 (in Fig. 1), we have removed the foreground galactic star located slightly off the center of the galaxy.

– **Tololo 1937−423** (North down, East right): this peculiar galaxy has lozenge isophotes. The central bright core contains a stellar nucleus of color $B-R \sim 0.6$ and exhibits protruding radial extensions. The external envelope is also blue ($B-R \leq 1.0$). The surface brightness distribution is fitted by a $r^{1/4}$ law.

3.6. The surface brightness distributions

In Paper I, we concluded that the 23 BCDGs from the Byurakan Surveys could be subdivided in three groups according to their surface brightness distribution: 10 objects clearly dominated by a "spheroidal" component fitted by a dominant de Vaucouleurs ($r^{1/4}$) law, 7 objects clearly dominated by an exponential brightness distribution, and 6 composite or unclassifiable profiles. With this limited northern sample, we found that about 3/4 of our objects belong to the two first categories.

In the present sample, we find a similar repartition of our BCDGs in the three groups just defined: 12 objects are dominated by an exponential component (7 are fitted by a pure exponential law), 12 are dominated by a $r^{1/4}$ law (5 are fitted by a pure $r^{1/4}$ law). By "pure" we mean that no other significant component has to be added to account for all the light of the galaxy. For the total sample of 44 Northern and Southern galaxies (1 companion included), we find that: 11 galaxies (25%) have SB profiles following closely a pure exponential distribution, and 8 (18%) galaxies with composite profiles in which the exponential component dominates; 9 galaxies (20%) have SB profiles following closely a pure $r^{1/4}$ distribution, and 12 galaxies (27%) with composite profiles in which the $r^{1/4}$ component dominates; finally, 3 galaxies are unclassifiable (7%), those peculiar galaxies are Mk 1499, Mk 1131 and SBS 1331+493 (Paper I).

Therefore, we support that the global structure of BCDGs, traced by their projected luminosity density, is not different, in terms of dynamical components, from the global structure in normal galaxies where two main stellar populations dominate. Those components are thick disks (whose true axial ratio distribution remains to be determined in the disk dominated BCDG galaxian population, see Sung et al. 1998), and spheroidal components obeying the $r^{1/4}$ law (implying a significant degree of relaxation). The present 20 disk-dominated BCDGs will be used to derive tight constraints on the true axial ratios of the disks, this will be treated in a following paper. In any case, kinematical data are also necessary, in addition to

Table 6. $r^{1/4}$ galaxies; north and south samples

Object	A (B)	A (R)	$\mu_0(B)$	μ_0 (R)	Composite
Mk 996	9.57 ± 0.06	9.75 ± 0.09	13.50	12.12	
Mk 600	9.71 ± 0.07	8.16 ± 0.15	14.56	16.44	
Tol 0513−393	10.23 ± 0.23	11.83 ± 0.63	12.52	10.89	C
Tol 0645−376	10.03 ± 0.12	9.70 ± 0.15	14.13	13.26	
Tol 0957−279	10.09 ± 0.10	9.14 ± 0.20	11.97	14.06	C
Tol 3	9.50 ± 0.05	9.14 ± 0.06	12.72	11.45	C
Fairall 6	11.59 ± 0.24	10.59 ± 0.60	10.08	9.34	C
II SZ 34	10.81 ± 0.09	9.74 ± 019	13.07	14.48	
13209-2329	9,.438 ± 0.08	9.69 ± 0.11	13.02	12.39	C
Tol 1434+032	9.23 ± 0.12	9.17 ± 0.12	15.86	15.38	C
Tol 1448+116	– ± 10.383	0.10 ± –	13.28	C	
Tol 1924−416	10.27 ± 0.08	9.29 ± 0.08	10.42	10.87	
Tol 1937−423	10.32 ± 0.06	10.20 ± 0.04	12.51	11.82	C
SBS 0136+328	9.62 ± 0.10	9.38 ± 0.07	14.15	13.23	C
SBS 1054+504	9.32 ± 0.07	8.92 ± 0.11	13.08	12.90	
SBS 1147+520	9.98 ± 0.16	8.23 ± 0.11	12.66	13.42	
Mk 324	13.14 ± 0.50	9.58 ± 0.07	11.23	11.17	C
Mk 1434	9.08 ± 0.11	8.85 ± 0.05	12.88	12.04	C
Mk 1450	9.62 ± 0.09	9.79 ± 0.08	12.08	9.99	
Mk 1480	9.87 ± 0.14	9.16 ± 0.08	12.16	12.55	C
Mk 1418	10.19 ± 0.40	9.88 ± 0.09	11.53	10.49	C
Mk 1426	– ± 8.92	0.09 ± –	11.82		

photometry of a larger sample of objects. Regarding the dynamics of the BCDGs, both exponential and $r^{1/4}$, we insist that a deeper analysis requires kinematical data from the gas *and* stellar populations.

The use of the light distribution to trace the mass distribution can be done to some extent, keeping in mind that the mass-to-light ratio usually varies within the galaxies, as indicated by the color gradient in BCDGs (Papaderos et al. 1996b; Doublier et al. 1997 and this work). The central starburst dominated regions have mass-to-light ratio close to 0.1 (Charlot et al. 1996) in the visual, while the outer old star population dominated regions (Thuan 1983; Hunter & Gallagher 1985; Doublier et al. 1999) would have a mass-to-light ratio larger than 1. As a result, the mass distribution would flatten towards the center compared to the light distribution. Nevertheless, studies of the light profile in the near-infrared (Doublier et al. 1999) shows that BCDGs with "optical" $r^{1/4}$ law profiles display $r^{1/4}$ law profiles in the K band where the old stellar population dominates without a light excess in the central parts. This leads us to believe that the $r^{1/4}$ law is intrinsic, rather than being due to the light excess caused by the presence of the star formation regions.

In Tables 5 and 6, we summarize the parameters derived from our photometric analysis. The surface brightness profiles were fitted uniquely either by a $r^{1/4}$ law or an exponential law. If neither case applies, a note in the last column of Tables 5 and 6 mentions that the surface brightness is "composite".

The parameters of the exponential law and of the de Vaucouleurs ($r^{1/4}$) law were estimated using a crossed-linear regression applied to the regions that were not affected by the central "bulge-like" component (in case of the exponential law) and seeing (in case of the de Vaucouleurs law), and excluding the outermost isophotes where the signal-to-noise ratio is too low. In a following section, we discuss the "extra" components such as the central excess of light, or any possible excess of light present in the low S/N regions of the galaxies.

The excess of light in the central regions is probably due to the star forming regions: the method described by De Vaucouleurs (1959) we used to derive our surface photometry defines the center as the photometric center, while for ellipses fitting of the isophotes the center of the galaxy is defined as the center of last inner ellipse. We have tried the ellipses fitting on some of the most clumpy BCDGs in our sample, and the results are sensibly in agreement (within a few percent) in the outer regions, while the fit diverge considerably in the central regions.

The excess of light compared to a pure exponential law, or to the de Vaucouleurs law, seen in the outer parts of some BCDGs is not likely due to large errors (see surface brightness distributions in Fig. 1). In some cases, it could be attributed to an old, very low surface brightness component, whether this component could be exponential or $r^{1/4}$ is not clear. This component is detected in few cases (UM 465A, Fairall 301) in the near IR (Doublier et al. 1999).

Figure 2 displays the surface brightness distributions of the $r^{1/4}$ BCDGs in the $[\mu, (r/r_{\rm eff})^{1/4}]$ plane, where μ is the surface brightness in mag/arcsec^2, and $r_{\rm eff}$ the effective radius defined in Sect. 3.3.1 (a similar plot can be found in Paper I, for the northern sample). The plotted line represents the relations between the reduced radius and the surface brightness for a pure de Vaucouleurs law. Most of the $r^{1/4}$ profiles show a much steeper slope than the de Vaucouleurs relation. We discuss this difference in terms of the surface brightness gradient in the next section.

3.6.1. "De Vaucouleurs" profiles (23%)

Figure 3 (top panel) shows the relation between the observed slopes of the $r^{1/4}$ laws in reduced coordinates in R and B. The slope values are systematically larger than the canonical value of 8.327 for the law. Furthermore, the slopes are clearly larger in B than in R. This was also observed in our northern sample (Doublier et al. 1997) for which we suggested either having systematically overestimated the effective radii or the presence of an homogeneous component in addition to the dominant spheroid. The systematic *excess* over the 8.327 value and the fact that this excess is larger in B than in R leads us to conclude that the presence of the starburst "component" is probably responsible for this effect.

The most natural explanation is that the effective radius is overestimated. The overestimation of $r_{\rm eff}$ could result from errors in extrapolating the asymptotic magnitudes; however, we performed the surface photometry

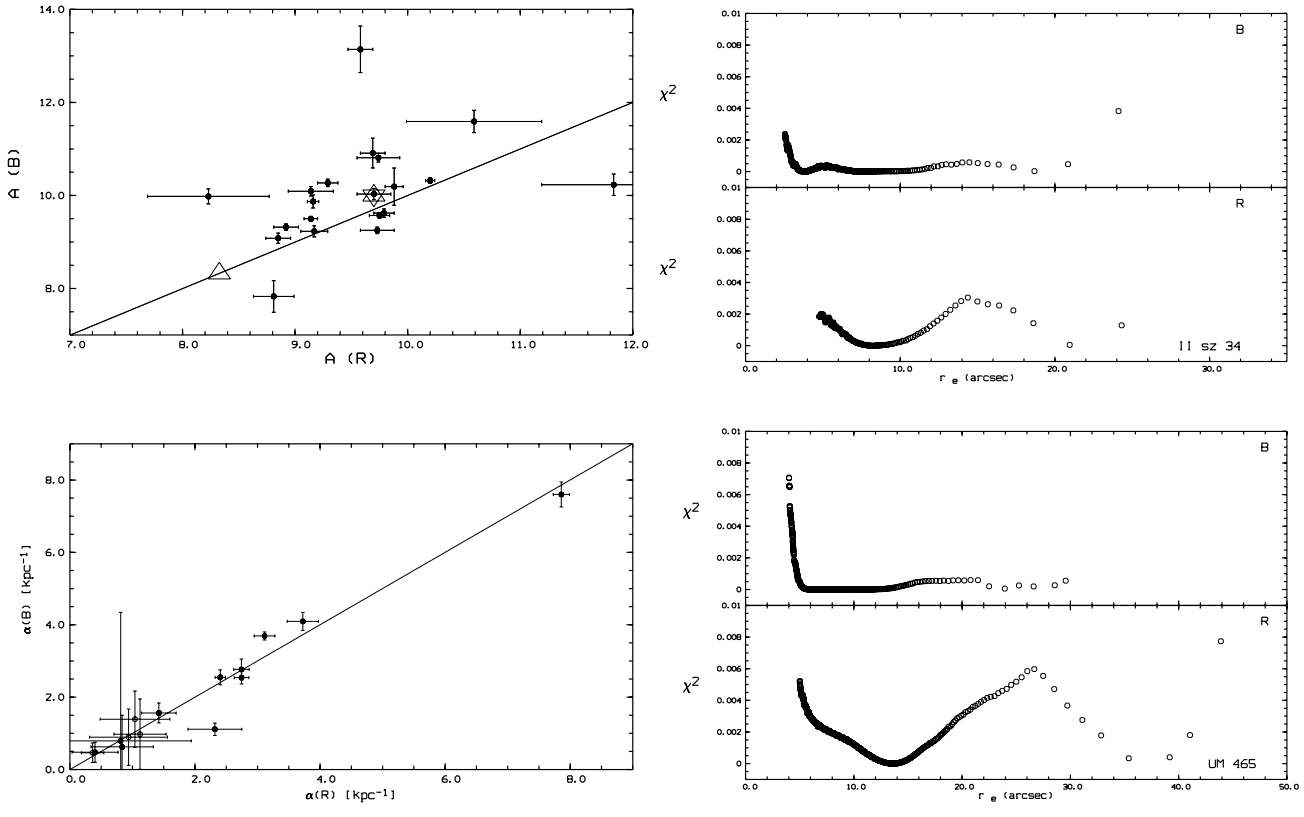

Fig. 3. Relationship between the scale-length in B and R band. **a)** Relationship between de Vaucouleurs law slopes. The solid line represents the line of equal slopes in B and R. The relationship is obviously steeper than 1, the coefficients are systematically larger in B than in R, and systematically larger than the usual value 8.327. The large star represents the mean values of the subsample (10.0 in B and 9.7 in R) while the large triangle shows the empirical values of 8.327 in both bands. **b)** Relationship between the scale-lengths of the disk galaxies (or composite when the disk was easy to separate) in B and R bands. The solid line represents the line of equal scale lengths in B and R. The scale-lengths in both colors are clearly correlated. **b, c)** Variation of the χ^2 as a function of the Equivalent. Radius. **b)** Variation of the χ^2 for the elliptical-like galaxy: II SZ 34. The χ^2 was obtained by dividing the surface brightness distribution modeled by the best fitting $r^{1/4}$ law, by the observed surface brightness distribution. Note the local maxima, in B and R, corresponding to inner features of the galaxy. **c)** χ^2 variation for the disk galaxy: UM 465, obtained in the same way as above. Note the local maxima of the χ^2 that are, unlikely to the elliptical case, behaving differently in B and R

several times showing that the internal consistency of the asymptotic magnitude values is good. Then the excess $r_{\rm eff}$ values could result from the presence of a small compact component of a small scale length in the central part of the BCDG.

To investigate this hypothesis, we have simulated 3 types of galaxies: a pure elliptical, a dominant elliptical with a small additional $r^{1/4}$ central component, and a dominant elliptical with a small exponential central component. Seeing effects have been added by means of a convolution of the model galaxies with a Gaussian. The model images have subsequently been submitted to the surface photometry procedure, yielding a clear tendency to overestimate the resulting $r_{\rm eff}$ of the "Host galaxy + Starburst component" whatever the nature of the starburst component.

To check the consistency of the fit to the $r^{1/4}$ law, we have performed χ^2 tests by subtracting the model $r^{1/4}$ SB distribution that best fits from the observed SB. Figures 2b and 3c displays, as an example, the results on Mk 996 and II SZ 34 in B and R. The value of χ^2 for II SZ 34 shows local maxima at 5, 15 and 30″ from the center, implying local significant departures from the pure $r^{1/4}$ law in these regions. These local departures originate from the fact that not all the star formation regions are concentrated in the central parts of the galaxies. This is commonly encountered in almost all "spheroidal" BCDGs of our sample.

3.6.2. Exponential profiles (25%)

The mean value of the scale length parameter is 1.63 $\rm kpc^{-1}$ without taking into account the scale length value of the first component of UM 461 (7.57 ± 0.1 ($\rm kpc^{-1}$)) that may be due to the two very bright nuclei.

Figure 3 (bottom panel) shows the relation between the scale length in B and R. The relation shows that the scale lengths in B and R are well correlated. The disks should have similar stellar distribution in R and in B. In some cases, the B scale length is significantly larger than the R scale length.

Figures 3b and 3c show the χ^2 variation for UM 465A, as a function of the equivalent radius, in B and R. As for the de Vaucouleurs profiles, the χ^2 show small variations larger than the mean scale length that account for the existence of small structures within the disk of the galaxy: off-centered star formation regions, foreground faint stars, and globular clusters.

The disks and de Vaucouleurs parameters describing the galaxies are listed in Tables 5 and 6 respectively.

3.6.3. Composite profiles

We call "composite" SB profiles that cannot be fitted by a pure exponential or a pure $r^{1/4}$ law. The shapes of these profiles (in B and R) can be very different from one galaxy to another. In most cases, two components are easily seen, the observed profiles being the sums of an exponential and a $r^{1/4}$, as in giant spirals, with one of these components being more or less dominant. However, for some other galaxies, the profiles displayed in the [r_e, μ] plane show a convex shape but when displayed in the [$r^{1/4}$, μ] plane, the profiles exhibit a concave shape. Also, these galaxies show very disturbed isophotes. These systems may be relaxing merger remnants, or they could have a thick disk not yet settled inside a host elliptical galaxy.

4. Discussion

Hereafter, we discuss the properties of our complete sample of northern and southern galaxies. This accounts for 44 objects, including the UM 465 companion. Five objects are not "dwarfs" according to the criterion of having a luminosity $M_B \geq -16.5$: SBS 0136+328, Tololo 0513−393, Tololo 0645−376, Tololo 1924−416, and Tololo 1937−423. These brighter galaxies are included in the discussion to compare with our low-luminosity star-forming galaxies. The companion of Tololo 1924−416 is not included. We assume $H_0 = 80$ km s^{-1} Mpc^{-1} for the derivation of distance-dependent quantities based on the Galactocentric corrected recession velocities. Table 7 summarizes the absolute parameters: absolute magnitudes and linear radii, for the southern sample (see Paper I, for the Northern sample values).

Table 7. Absolute magnitudes and linear radii

Object	d [Mpc]	M_B	$r_{\rm eff}$[pc](B)	r_{26}[pc](B)
			$r_{\rm eff}$[pc](R)	r_{26}[pc](R)
Haro 14	12.1	−16.50	716	2103
			712	2586
Mk 996	20.4	−16.21	717	2349
			795	3115
UM 417	33.3	−14.51	83	1110
			79	1600
Mk 600	12.6	−15.03	474	921
			856	1626
Fairall 301	8.5	−15.50	434	1622
			455	2072
Tol 0513−393	179.6	−17.66	1692	3367
			1692	4990
Tol 0610−387	18.8	−15.35	941	1882
			2008	4449
Tol 0645−376	91.5	−17.97	2557	5388
			2330	7515
Tol 0954−293	25.7	−16.26	623	2131
			550	2360
Tol 0957−279	5.2	−14.52	209	910
			712	1495
Tol 3	10.8	−16.07	459	1772
			465	2970
Fairall 6	23.9	−15.82	504	1823
			579	2497
UM 461	8.9	−13.58	256	606
			311	819
UM 465	11.4	−15.91	394	1698
			520	2103
UM 465b	11.4	−13.51	482	953
			452	917
I SZ 59	19.0	−16.12	791	2616
			1466	4154
I SZ 399	8.5	−15.15	244	1343
			275	2125
II SZ 34	32.6	−16.29	872	2251
			2367	6413
13209-2723	29.8	−16.30	564	2114
			832	3652
Tol 1434+032	16.1	−14.61	975	1509
			1361	2652
Tol 1448+116	23.0	−14.98	743	1155
			831	2152
Tol 1924−416	34.7	−18.29	752	3960
			849	4014
Tol 1924−416b	34.7	−14.93	2309	1895
			2537	2598
Tol 1937−423	32.6	−17.14	1098	3326
			1116	4435

4.1. Color distribution

The asymptotic mean $B-R$ color of the present sample is 1.13 ± 0.35, consistent with that reported for the Northern sample ($B-R = 1.07 \pm 0.09$). The spread in asymptotic color for the southern sample is due to the fact that we have redder objects, and that our photometry is deeper in R band - therefore we reach the reddest parts of the galaxies. The observed colors span the range 0.34 to 1.63. We have one object bluer than 0.5, Tol 0954−293, an exponential–dominated galaxy. Figure 4a shows the distribution of the $B-R$ color for the 41 objects with mean and median $B-R = 1.1 \pm 0.4$.

Figure 4b shows separate color distributions for the three main surface brightness profile types. The average $B-R$ colors are: 1.32 ± 0.4 for the $r^{1/4}$ BCDGs, 1.10 ± 0.2 for the exponential BCDGs and 1.09 ± 0.3 for the composite profile BCDGs (composite $r^{1/4}$:

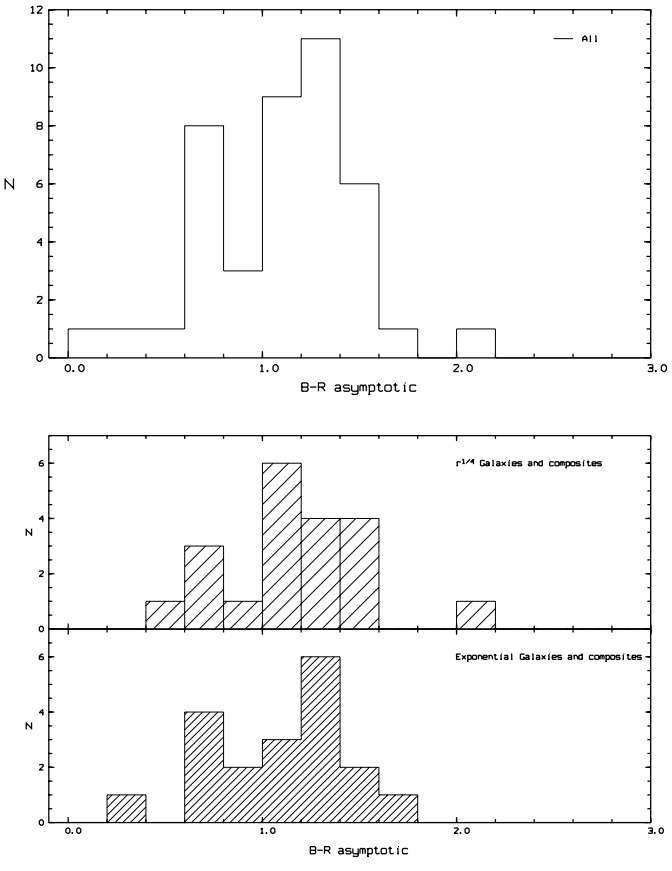

Fig. 4. $B-R$ color distribution. **a)** $B-R$ asymptotic total color distribution for the whole sample (44 galaxies) in solid lines. **b)** $B-R$ color distribution as a function of the galaxy type. The top box shows the distribution for the elliptical-like objects, the bottom box shows the distribution for disk galaxies (dash) and for composite profile galaxies (solid line)

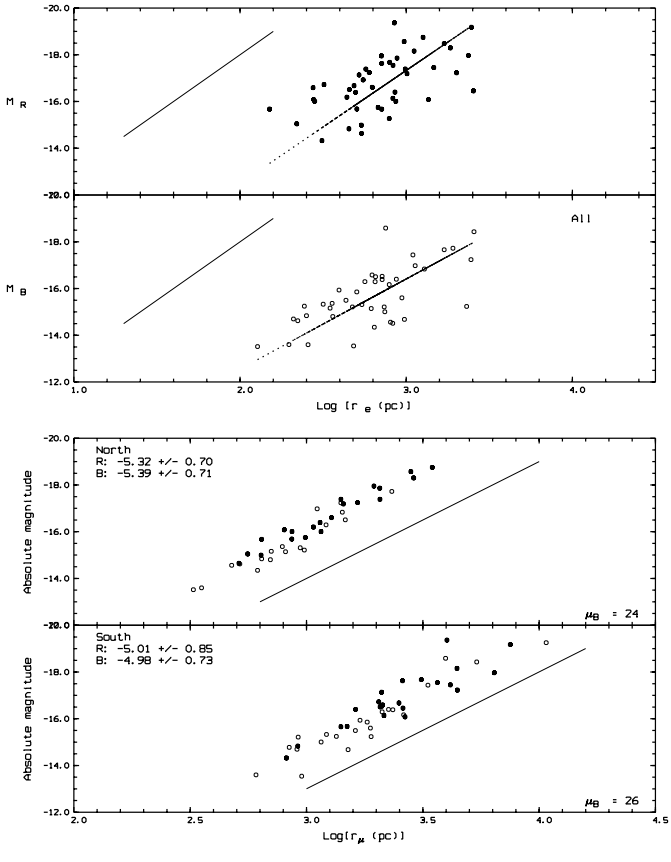

Fig. 5. Luminosity–Radius relationship. **a)** Relationship between the effective radius in B and R, and the absolute magnitude for the whole sample. The solid line has a slope of -5 and the dashed line represents the least-square fit to the data. **b)** Relationship between the absolute magnitude in B (empty circle) and R (filled circle) but using 2 different isophotal radii: at $\mu = 24$ B mag/arcsec^2 from the sample in Paper I (top), and $\mu = 26$ B mag/arcsec^2 from the present sample (bottom). The solid line has a slope of -5

$B - R = 1.08 \pm 0.3$, and exponential composite: $B - R = 1.09 \pm 0.4$).

There is a tendency for the pure $r^{1/4}$ BCDGs to be redder than the exponential ones. However, composite profile objects have the same average asymptotic color as the pure exponential ones, whatever the nature of the dominant component.

4.2. Radius-luminosity relations

Figure 5a shows the relation between the effective radius in pc and the absolute magnitude (corrected for foreground Galactic absorption). We confirm the findings of Paper I, that there is a tendency for the observed relation to depart significantly from the expected relation:

$$M_{\rm abs} = -5 \times \log r_{\rm e} + C^{\rm st}. \quad (6)$$

The observed slopes are -3.86 ± 1.13 in B, and -4.84 ± 1.48 in R. After a 1-sigma rejection iteration, the slopes become -3.72 ± 0.9 in B and -4.45 ± 0.9 in R. The departure from the empiric relation is clear in B but there is a large scatter in the data. Part of this scatter may be due to errors in the extrapolation process used to derive asymptotic magnitudes and effective radii. In Paper I, we have already explained this effect in terms of a selection bias towards compact and centrally located starbursts inside our galaxies.

In the R band, there is no significant difference between the empirical value of the luminosity–radius relation and the observed value for our sample. This is due to the fact that the starburst does not dominate in the R band (except if H_α dominates the spectrum, the effect would then be similar to the compactness bias, but smaller and lost in the scatter due to magnitude errors), causing the properties of the "host" galaxy to dominate.

Figure 5b shows the relation between the absolute magnitude and the isophotal radius at $\mu = 26$ mag/arcsec^2 for the present sample. For comparison, we have also reproduced the corresponding plot from Paper I, but at $\mu = 24$ mag/arcsec^2. The values of the slope are not

significantly different from the empirical value of −5. At these low levels of surface brightness, the dominant component is obviously the underlying galaxy. If the underlying galaxy of the BCDGs is composed of evolved stars of several Gyrs (i.e. if the scatter in the mass-to-light ratio is small; Thuan 1983; Hunter & Gallagher 1985; Doublier et al. 1999), the intensity at a given radius is proportional to the stellar volume density integrated along the line of sight. The scatter is much reduced indicating that the stellar overall density properties of the host galaxy may be quite similar for all BCDGs.

4.3. Compactness

The compactness of a galaxy is a visual impression translating a combination of small angular size and "high" surface brightness. Therefore, to provide quantitative estimators of compactness, one is led to use the value of some quantity resulting from a combination of these observables. Two such indicators are discussed in the following:

The mean surface brightnesses are measured inside a given "metric" radius (as compared to the sky brightness, around 22 mag arcsec^{-2} in B band, 21.5 in R band), which we choose to be the effective radius. For our total sample, the average value of the effective mean surface brightness is 21.6 ± 1.2 mag arcsec^{-2} in B band (corrected from Galactic extinction). Note that this is slightly brighter than the canonical central value of the surface brightness of giant disk galaxies derived by Freeman (1970), but compares well with Papaderos et al. (1996a) derived from their BCDG sample. It translates into an apparent projected luminosity density on the line-of-sight of 150 $L_\odot$ pc^{-2}.

Figures 6a and b show that there is a marked difference between the exponential objects and the $r^{1/4}$ ones. The latter have a symmetric distribution around $< \mu_{\rm eff} >$ = 21.03 ± 0.9 mag arcsec^{-2} (238 $L_\odot$ pc^{-2}) while the exponential dominated galaxies have a very flat distribution of mean effective brightness with $< \mu_{\rm eff} > = 22.2 \pm$ 0.9 mag arcsec^{-2} yielding a clearly fainter 87 $L_\odot$ pc^{-2}. Among composite objects, those dominated by a $r^{1/4}$ are one magnitude brighter in average than those dominated by an exponential.

Figures 7a and b show the distribution of the distance independent concentration index defined by the ratio of the effective radius to the radius containing 1/4 of the total luminosity (De Vaucouleurs & Aguero 1973; Fraser 1977). Another compactness index has been used by Papaderos et al. (1996b): it is based on the ratio of the starburst component projected area to the total area of the galaxy seen at the isophote 25 mag arcsec^{-2} in B; it was derived from the profile decomposition for a sample that exhibits a "plateau" component in B, presumably caused by the starburst population. We have not used this

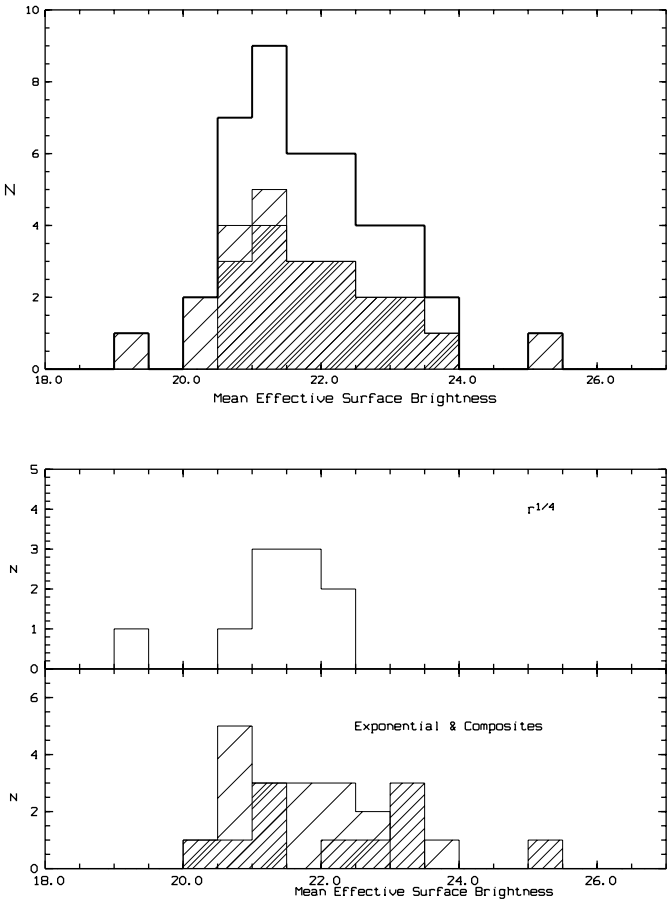

Fig. 6. Mean Effective Surface Brightness Distribution. **a)** Distribution of the mean effective surface brightness for the whole sample (solid line), the Northern sample (short dash) and the Southern sample (long dash). **b)** Mean effective surface brightness distribution for different galaxy types. Top: $r^{1/4}$ dominated BCDGs, bottom: exponential dominated BCDGs (long dash), and composite profile BCDGs (short dash)

definition, because very few of our BCDGs profiles exhibit such a clear-cut plateau allowing a three-component decomposition. James (1991) or Doi et al. (1995) use concentration index definitions that are basically similar to de Vaucouleurs' definition.

Figure 7a shows the distribution of the concentration index (CI) in B and R displayed on the same graph for comparison. The mean values in B and R are very similar with a value of 2.25 ± 0.5, that is larger than the value we obtained for the northern sample. We should note that the southern sample contains slightly more luminous BCDGs. The CI in B and R are basically consistent, but their correlation coefficient is low, only 0.5. Our observations in the near-infrared will allow to extend the study of the CI to J, H and K bands that are in principle more sensitive to the underlying evolved stellar populations.

Figure 7b shows the distribution of the CI for the disk BCDGs and the elliptical BCDGs in both B and

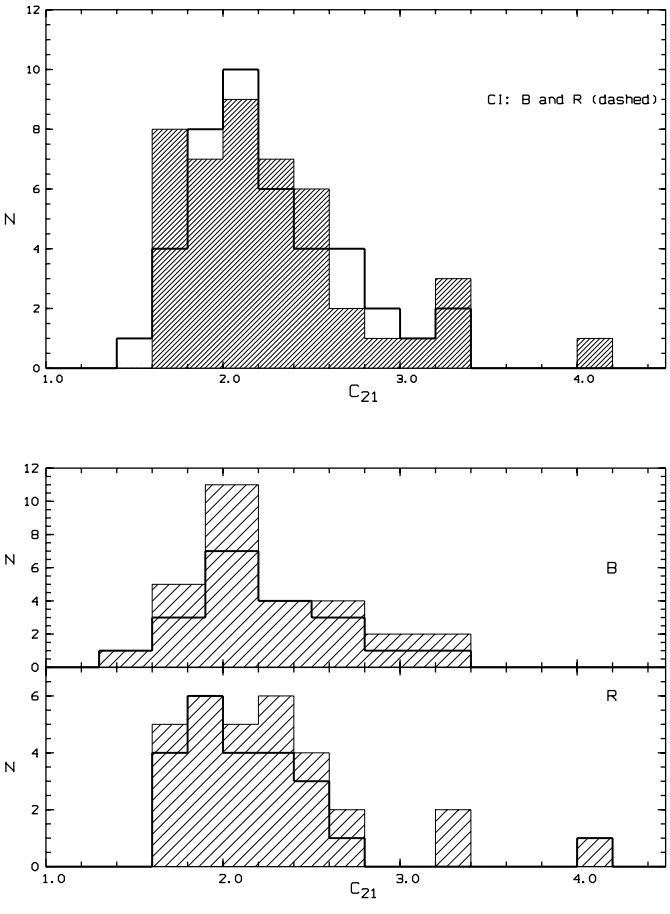

Fig. 7. Concentration Index distribution. **a)** Concentration index distribution in B band (solid line), and in R band (dash). **b)** C_{21} distribution for two galaxy types: elliptical-like BCDGs (dash) and Magellanic-like BCDG (solid line), in B (top) and R (bottom) bands. In B, the elliptical-like are more compact than the disk-like ones. There is no difference in R

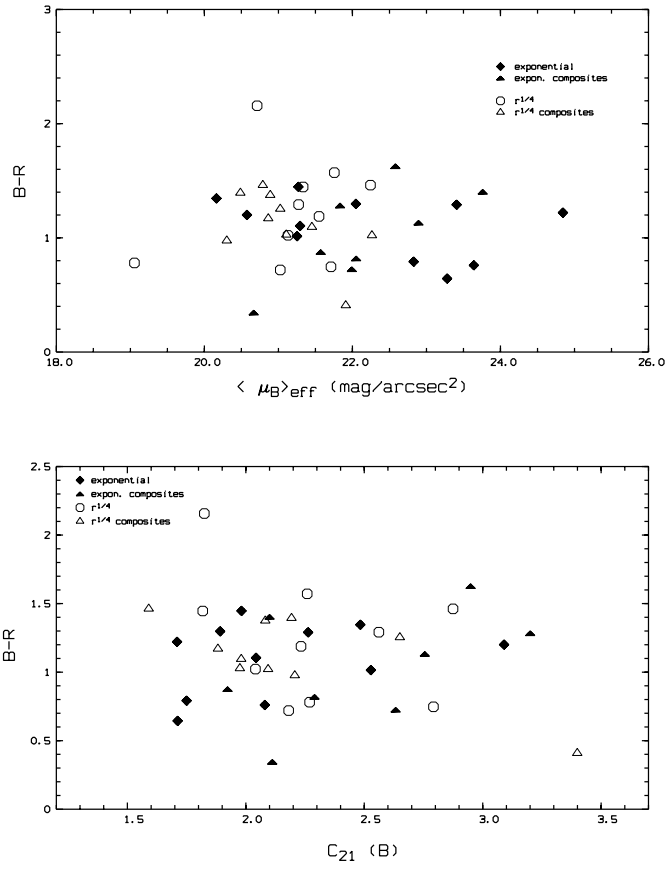

Fig. 8. "Compactness" indexes versus Asymptotic $B-R$. **a)** Mean surface brightness in B band versus asymptotic $B-R$ for the 4 photometric classes of BCDGs. **b)** Concentration index C_{21} versus asymptotic $B-R$ for the 4 photometric classes of BCDGs

R bands. The CI is similar for the exponential galaxies (2.27 ± 0.5 in R and B) and for the $r^{1/4}$ (2.25 ± 0.1 in B and R). There is a slight difference between the pure $r^{1/4}$ (CI(B) $= 2.3 \pm 0.3$) and the pure exponential dominated BCDG (CI(B) $= 2.1 \pm 0.4$), but the scatter remains large and it is difficult to conclude.

Let us underline that the two compactness indicators studied above do not pertain to the same physical quantities. The concentration index is a dimensionless number that is the ratio of two metric radii, physically associated with the scale length of the projected brightness distribution, regardless of any assumption on the shape of the surface brightness distribution. On the other hand, $< \mu_{\rm eff} >$ which is a logarithmic projected luminosity, is rather directly linked to the visual aspect of the central region of the galaxies. The differences in compactness interpretation are illustrated in Figs. 8a and 8b in which $C_{21}(B)$ and $< \mu_{\rm eff} >$ are plotted versus the asymptotic $B-R$. Obviously $< \mu_{\rm eff} >$ is not correlated with $B-R$ whatever the photometric type of the BCDGs (elliptical-like, disk-like or composite). On the contrary, CI(B) exhibits a weak correlation (t-coefficient of Student's test: 9.54, with a probability of exceeding this value of 10^{-11}) with $B-R$ for exponential dominated objects only. This correlation almost vanishes for the $r^{1/4}$ dominated BCDGs, even when Mk 324 and Mk 1450 deviant values are included.

It is tempting to interpret this as a result of differences in the evolutionary history of the two photometric classes of BCDGs: disk-dominated systems evolving possibly with recurrent bursts due to accretion of HI clouds but keeping their overall dynamical structures and hence their basic scale length parameters, while the elliptical-like BCDGs would be the products of violent dynamical events that bring fundamental changes in their structure: merging, interaction with an HI cloud, or a larger galaxy.

However, it might be that the concentration index depends strongly on the presence of the starburst, since the mean $B-R$ color ($< B-R >_{\rm eff} = 0.65 \pm 0.12$) within the effective radius is much bluer than the integrated $B-R$ color by 0.4 mag. It is most likely, once the starburst has faded, that the concentration index will change,

i.e. decrease significantly as the light density decreases. Thus, the differences we see for the C_{21} might disappear after the BCDG phase.

Table 8 summarizes the average values of some photometric parameters for the two BCDG populations of our sample.

4.4. Blue neighbours and companions for BCDGs

The study of the environment of HII galaxies reported by Telles & Terlevich (1997) showed that less than 10% of these galaxies (including BCDGs) have larger companions (normal, giant galaxies within a cylinder of 200 km s^{-1} in depth and a hundred kiloparsec in projected radius). A recent study of Pustil'nik et al. (1995) showed also that the dwarf emission line galaxies of the Second Byurakan Survey do not show any clustering tendency within regions of more than 5 Mpc^{-3}. The BCDGs selected for observation in the present work have no neighbouring larger units. Except for Mk 1308, Mk 1480 and Mk 1481, and II SZ 34, our objects are "isolated". However, galaxy formation theories using hierarchical models predict that the bulk of the galaxy population formed out from proto clouds of small mass (Kauffmann et al. 1997). Indeed, if the BCDGs, as isolated as they appear to be, have formed out of density fluctuations independent from the larger ones responsible for the formation of giant spirals and ellipticals, the power spectrum associated to these fluctuations implies that these BCDGs should be surrounded by smaller mass units, somehow larger than globular clusters, like fragments or galactic debris. Although merging should have happened frequently among the debris, some of them might still be found around the BCDGs.

Following this argument, we examined our frames closely, in B, R and especially the $B-R$ maps. We could detect ($S/N > 10$ in R, S/N[1] ~ 3 in $B-R$) some extended ($FWHM \geq 1.5''$, with a seeing $\leq 1''$) objects with $B-R$ colors ranging from 0.5 to >3. Among these, we selected the objects showing the "bluest" colors: 0.5−2.0, in order to sort out the closest ones, therefore with lowest k-correction. Only few objects in the fields met the requirements, and the selection was done visually using the $B-R$ maps. Selecting out blue stars was straightforward: when we constructed the color maps, we did not take into account the slight variation of the PSF from one filter to another, as the differences are not significant for extended objects. But they are, indeed, clearcut on the star images: on the $B-R$ maps, the stars show a wavelet (or "sombrero") profile due to the difference in the PSF shape (the seeing is generally worse in B than in R). For the faintest stars, the PSF differences are not significant and therefore one has to check directly the $FWHM$. We set a lower limit of $4''$ on the size of the detected objects assumed to be "extragalactic blue sources", to avoid effects due to image aberrations.

[1] The value refers to the ratio between the "mean $B-R$" inside the object to the rms.

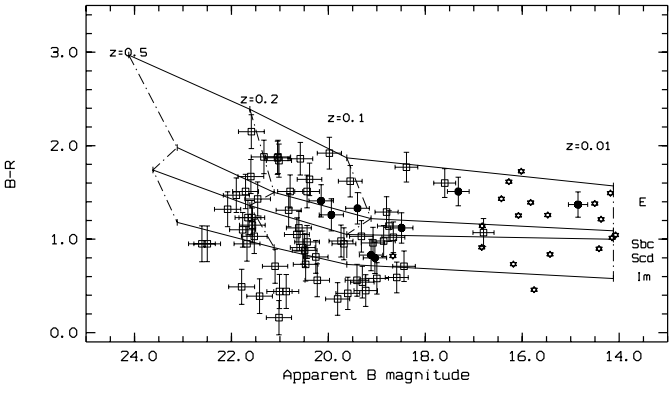

Fig. 9. Apparent B magnitude versus $B-R$ color diagram for faint extended objects observed in the neighbourhood of BCDGs. See detailed explanation in the text (Sect. 4.4)

Figure 9 shows the $B-R$ colors vs. apparent B magnitude diagram of the selected objects with our BCDGs for comparison, and summarizes how we define "candidate" companions. The overplotted lines represent the variation of the [magnitude, color] location of different galaxy types with redshift (derived from Frei & Gunn 1994 (FG94), and Pence 1976 (P76)). First of all, we followed P76's tracks establishing the values of the apparent magnitudes for different galaxy types (E-S0, Sbc, Scd and Im: $H_0 =$ 75 km s^{-1}/Mpc) at the various redshifts given by FG94 (including K-correction) in the B band. From FG94, we derive $B-R$ colors at a given redshift for apparent B magnitudes of various galaxy types. Most selected objects (empty squares) fall beyond the redshift of 0.1, and therefore are probably background galaxies. Indeed, almost all of them appear on the frames to lie in "groups" close (few $10''$) to a much redder object (≥ 3). Likely, in these cases, we are detecting late type galaxies in small clusters or groups.

For the few objects suspected to be at low redshift ($z \leq 0.1$) from their position in the [magnitude, color] plane, in term of absolute values, their sizes range between $5''$ and $20''$ in diameter, i.e. 10 − 40 kpc (at $z = 0.1$) or 1 − 4 kpc at $z = 0.01$ (highest redshift of the BCDGs in our sample). We are thus led to speculate whether these objects are background late type galaxies, or physical "neighbours" of our BCDGs (stars). The apparent magnitudes range from $B = 24$ to 17 mag i.e. $M_B = -9$ to -16 at $z = 0.01$ and -14 to -21 at $z = 0.1$. Only if the redshift is 0.1 or larger, the objects would lie in the luminosity range of the Scd and Sbc; indeed, a few "large" objects do show some inner structures very close to those of spirals or large irregulars when seen face-on. For smaller redshifts, the objects would lie in the "dwarf" zone ($M_B \geq -17$).

In the fields, we found a population of objects that lies below the line defined by the Im galaxies in terms of color (Fig. 9). We do not have redshift measurement to

Table 8. Average values of photometric parameters

	N° of objects	$< \mu_{\rm eff} >^*$ B mag/arcsec^2	$< r_{\rm e} >^*$ pc	$< I_{\rm e} >(B)$ $L_{\odot\ B}$.pc^{-2}	$< I_{\rm e} >(R)$ $L_{\odot\ R}$.pc^{-2}	$< B-R >^*$
$r^{1/4}$ dominated	21	21.03 (0.67)	720 (608)	254^{469}_{134}	156^{237}_{68}	1.17 (0.40)
Exponential dominated	18	22.20 (0.9)	640 (287)	87^{198}_{38}	71^{196}_{26}	1.08 (0.26)

(*): Standard deviation for the subsample considered.

identify their origin. Only 3 of them have diameters of 4″ and could be faint blue stars, but all others have diameters larger than 8″ and could not be mistaken for stars.

The galaxies identified with filled circles are objects found close to the BCDGs ($\leq$ 20″ from their outermost isophotes) with a low average surface brightness ($< SB >_B \sim 25.5$ mag arcsec^{-2}). These objects are likely to be companions because they are not associated with other galaxies in the fields except the nearby BCDG; they do not show marked internal structures. Most interesting, 4 of them (in the field of Tol 1924−416, Tol 0610−387, Mk 600 and UM 461) seem to lie in the direction of the distortions seen in these BCDGs. As seen in Fig. 9, these objects lurk across the area populated by other galaxies and do not define a specific sequence.

Östlin et al. (1998) recently confirmed the association between Tololo 1924−416 and the faint blue companion located NE of this galaxy. This result strengths our hypothesis that some of our faint neighbours could be indeed companions.

Moreover, recent studies using HI mapping around BCDGs and other Low Surface Brightness Dwarf galaxies, showed that many of them do have "HI" companions that have no detected optical counterparts on deep plates ($<$ 50%, Taylor et al. 1994; Taylor et al. 1995; Taylor et al. 1996). It would be worthwhile to search for HI companions around our BCDGs. It would also be of interest to compare the spatial distribution of the faint optical companions.

More observations, among which, obviously, redshift determinations, are needed to ascertain the physical association of these candidates with the BCDGs.

5. Tentative evolutionary scenario

Over the past few years, some evolutionary scenarios have been proposed in order to place the BCDGs and the other types of dwarf galaxies, dEs and dIs, into an unified scheme. Lin & Faber (1983), Davies & Phillipps (1988) have proposed in view of the morphologies and surface brightness distributions that dIs, and dEs might go through a BCD phase. This star formation phase can happen in dE providing that an important gas refueling has occured. The recent work of Sung et al. (1998), based on the comparison of the intrinsic shapes of BCDGs and dEs, dIs, shows that they present morphological similarities. Van Zee et al. (1998) show that HI properties differ largely from one type to another, with some BCDGs showing evidence of ongoing mergers (e.g. II ZW 40). BCDGs have more compact HI clouds, less clumpy than dIs. Finally, they show that the HI within BCDG is rotationally supported, with velocity gradients indicating, however, more complex kinematics, while dEs are most probably not.

The main difficulty of classifying the BCDGs in an evolutionary sequence with both dEs and dIs, and to some extension with the Low Surface Brightness dwarf galaxies (LSB, hereafter), will strongly depend on what component defines the main body of the BCDGs. From dynamical considerations, stars dynamics can be considered completely disconnected from the gas dynamics. Finding a rotating gaseous disk inside a galaxy does not make it a "disk galaxy" since gaseous compact disks, with some star formation, are also found in giants elliptical galaxies (Brighenti & Mathews 1997; Silchenko 1997; Miller et al. 1997).

Apparently, depending on the tracers used for pinning down the dynamics and evolution of BCDGs, we might end-up with different answers: HI and young stars studies make them similar to low surface brightness HII galaxies, while the morphological studies lead to connect them with dEs or dIs.

Another aspect of the evolution is the environement: dEs and dIs are found mostly in cluster of galaxies, usually associated with a larger elliptical or a spiral. BCDGs and LSBs are preferentially found at the very edge of those clusters or in the fields, isolated.

During our work, we found that the 44 objects, we observed, could be classified into 3 classes: BCDGs whose surface brightness profiles are best described by an $r^{1/4}$ law, others by an exponential law, and a significant fraction for which it is not clear which of these laws dominates. This classification is somewhat independent of the star formation regions, since we took great care of fitting the profiles away from the light excess due to the starburst. If the light profiles reflect their general dynamics, BCDGs may represent a class of its own, with the LSBs as possible progenitors.

6. Conclusions

In this paper, we have presented the surface photometric study of a new sample of 21 Blue Compact Dwarf

Galaxies, observed from the southern hemisphere, selected out from several lists. An atlas of isophotal maps and brightness profiles has been produced. From the profiles, we could classify the BCDGs into the same three groups as obtained in Paper I. The results of the Northern sample (Paper I) and of this Southern sample were put together, and we obtained:

- 23% (9 objects) of our BCDGs have brightness profiles consistent with a pure $r^{1/4}$ law valid for classical luminous spheroidal systems. These galaxies have generally smooth isophotes at all brightness levels (with two or three exceptions), and show one large unresolved star forming region. Many of them show obvious departures from axisymmetry as boxy isophotes, isophote rotation, off–centered "nuclei", or in few cases, double central components.
- 25% (10 objects) of our BCDGs have brightness profiles that can be described by a pure exponential law characterizing disk systems. These systems seem closely related to Magellanic irregular galaxies because their morphology shows less smooth isophotes at least in the central regions, and usually multiple star forming knots. Kinematical data are necessary to draw conclusions on the flattening of these systems.
- 45% (20 objects) BCDGs could be "classified" as composite because their brightness distribution profiles are neither described by a pure exponential law or a pure $r^{1/4}$ law only. Nonetheless, nine of them are dominated by an exponential law and seem to be low luminosity analogs of giant "disk+bulge" systems; 11 of them are dominated by a $r^{1/4}$ law, and are possibly low luminosity analogs of "disky ellipticals". But, three of them remain unclassified (Mk 1131, Mk 1499 and SBS 1331+493), showing irregular patterns in the inner parts surrounded by a regular envelope. Their brightness distribution is difficult to interpret in terms of standard laws.

The color distribution of the BCDGs is representative of a blue galaxy population with some very blue cases. Some BCDGs show very strong $B-R$ color gradients indicating the presence of a stellar population distinct from the starburst region. We note a color discrepancy between the elliptical-like BCDGs and the disk-like BCDGs. The latter types show a tendency to be bluer in average than the pure $r^{1/4}$ BCDGs, but composite profile objects blur the picture.

The luminosity-radius relationship was investigated. The selection bias towards objects with a centrally located burst that provides excess of light in the B band is still obvious in the data. This bias itself takes origin in the selection mode of the original catalogs, basically done on prism-objective plates.

The high median values of the mean surface brightness inside the effective radius, the significantly large mean value of the concentration index, and the average short scale length of the brightness distribution as measured by the effective radii demonstrate that our sample indeed contains "compact" dwarf galaxies in overwhelming majority. $r^{1/4}$ dominated objects have higher average $< \mu_{\rm eff} >$ compared to the exponential dominated ones, but the latter already are significantly brighter than normal disk galaxies. Exponential dominated BCDGs seem to have a concentration index slightly correlated with their asymptotic color.

The results of this study of a sample of more than 40 BCDGs are leading to a more general view of the BCDGs. The various relationships investigated in this article are together consistent with the hypothesis that the differences in the morphology relate to differences in the intrinsic properties. The elliptical BCDGs are redder but more compact than the disk BCDGs. A small, but not negligible fraction of the BCDGs show a very disturbed light distribution with bluer colors when compared to the whole sample of the BCDGs. Those BCDGs may have experienced a strong past interaction (but in this case, the other actor is not in the immediate neighborhood) or an on–going merging event, while the star formation trigger in the elliptical and in the disk galaxies may be less extreme and violent.

In the new sample, we did not find any new close pair of BCDGs, but many fields show faint extended objects with similar colors to those of the BCDGs. The most obvious case is Tololo 1924−416 with a blue nebulosity located $3'$ SE off the galaxy for which we present the surface photometry as well. Observations are planned to obtain the redshifts of candidate neighbours in order to identify any low luminosity physical companions. Moreover, a number of features observed in the BCDGs images may be linked to recent past interaction and/or on-going merging phenomena (boxy isophotes, asymmetric envelopes, double nuclei structures). It is still premature to draw a conclusion on the triggering causes of the starburst without additional spectro–imaging observations that are presently under progress.

Considering the photometric results obtained on the present sample, it appears more difficult to force all BCDGs back into the evolutionary perspective contemplated by different authors (Lin & Faber 1983; Davies & Phillipps 1988 and Silk et al. 1987; Papaderos et al. 1996a; Telles et al. 1997; Telles 1996). Using B and R surface photometry only, there is no obvious and un-confusing argument allowing to set up a unique evolutionary scenario because the picture of the BCDGs is too much dominated by the light of the on–going starburst. Elliptical-like BCDGs may evolve into nucleated dwarf galaxies, while disk-like BCDGs may end as dwarf spheroidal galaxies, but for the composite profile BCDGs, there is no way to tell.

In our view, there is much evolution within the subclass of the Blue Compact Dwarfs and they may constitute

a segregated category during the short time-scale events that are responsible for their properties. It is most probable that the ending fate of a BCDG does not lie in the fading of the starburst but in its final dynamical state.

Acknowledgements. The authors wish to thank the support staff at the La Silla Observatory for their help. V.D particularly wishes to thank G. Dudziak for obtaining the spectrum of Tol 0954−293 during his own observing run. The program was supported partly by the governmental grant of the Ministère de l'Enseignement Supérieur et de la Recherche in France, and by the Program of Pre-doctoral Fellowship at the European Southern Observatory.

References

Bergvall N., Olofsson K., 1986, A&AS 64, 469
Bohuski T.J., Fairall A.P., Weedman D.W., 1978, ApJ 221, 776
Brighenti F., Mathews W.G., 1997, ApJ 490, 592
Burkert A.M., 1989, Ph.D. thesis, Ludwig-Maximilians-Univ., Munich, Germany
Burstein D., Heiles C., 1982, AJ 87, 1165
Charlot S., Worthey G., Bressan A., 1996, ApJ 457, 625
Davies J.I., Phillipps S., 1988, MNRAS 233, 553
De Vaucouleurs G., 1959, AJ 64, 397
De Vaucouleurs G., Aguero E.L., 1973, PASP 85, 150
De Vaucouleurs G., De Vaucouleurs A., Corwin J.R., Buta R.J., Paturel G., Fouque P., 1991, in Third reference catalogue of bright galaxies (1991), p. 0
Doi M., Fukugita M., Okamura S., 1995, ApJS 97, 59
Doublier V., Caulet A., Comte G., 1999 (in preparation)
Doublier V., Comte G., Petrosian A., Surace C., Turatto M., 1997, A&AS 124, 405
Fairall A.P., 1977, MNRAS 180, 391
Fairall A.P., 1981, MNRAS 196, 417
Fehmers G., De Grijp M., Miley G., Keel W., 1994, A&AS 108, 61
Fraser C.W., 1977, A&AS 29, 161
Freeman K.C., 1970, ApJ 160, 811
Frei Z., Gunn J.E., 1994, AJ 108, 1476
Hunter D.A., Gallagher J.S.I., 1985, AJ 90, 1457
James P., 1991, MNRAS 250, 544
Kauffmann G., Nusser A., Steinmetz M., 1997, MNRAS 286, 795
Kinman T.D., Davidson K., 1981, ApJ 243, 127
Kruger H., Fritze-V., Alvensleben U., 1994, A&A 284, 793
Kunth D., Maurogordato S., Vigroux L., 1988, A&A 204, 10
Kunth D., Sargent W.L.W., 1986, ApJ 300, 496
Landolt A.U., 1992, AJ 104, 340
Lin D.N.C., Faber S.M., 1983, ApJ 266, L21
Loose H., Thuan T., 1986a, in Star Forming Dwarf Galaxies and Related Objects, p. 73
Loose H.-H., Thuan T.X., 1986b, ApJ 309, 59
MacAlphine G.M., Williams G.A., 1981, ApJS 45, 113
MacAlpine G.M., Lewis D.W., 1978, ApJS 36, 587
MacAlpine G.M., Lewis D.W., Smith S.B., 1977, ApJS 35, 203
Meurer G.R., Heckman T.M., Leitherer C., Kinney A.R.C., Garnett D.R., 1995, AJ 110, 2665
Miller B.W., Whitmore B.C., Schweizer F., Fall S.M., 1997, AJ 114, 2381
Östlin G., Bergvall N., Rönnback J., 1998, A&A 335, 85
Papaderos P., Loose H.H., Fricke K.J., Thuan T.X., 1996a, A&A 314, 59
Papaderos P., Loose H.-H., Thuan T., Fricke K., 1996b, A&AS 120, 207
Pence W., 1976, ApJ 203, 39
Pustil'nik S., Ugryumov A.V., Lipovetsky V.A., Thuan T.X., Guseva N., 1995, ApJ 443, 499
Rodgers A.W., Peterson B.A., Harding P., 1978, ApJ 225, 768
Saglia R.P., Bertschinger E., Baggley G., et al., 1997, ApJS 109, 79
Salzer J.J., MacAlpine G.M., Boroson T.A., 1989a, ApJS 70, 447
Salzer J.J., MacAlpine G.M., Boroson T.A., 1989b, ApJS 70, 479
Savage B.D., Mathis J.S., 1979, ARA&A 17, 73
Silchenko O.K., 1997, Astron. Reports 41, 567
Silk J., Wyse R.F.G., Shields G.A., 1987, ApJ 322, L59
Smith M.G., Aguirre C., Zemelman M., 1976, ApJS 32, 217
Storchi-Bergmann T., Kinney A.L., Challis P., 1995, ApJS 98, 103
Sung E.-C., Han C., Ryden B.S., et al., 1998, ApJ 505, 199
Surace C., Comte G., 1994, A&A 281, 653
Surace C., Comte G., 1997, Rev. Mex. Astron. Astrofis. Conf. Ser. 6, 102
Taylor C.L., Brinks E., Grashuis R.M., Skillman E.D., 1995, ApJS 99, 427
Taylor C.L., Brinks E., Pogge R.W., Skillman E.D., 1994, AJ 107, 971
Taylor C.L., Thomas D.L., Brinks E., Skillman E.D., 1996, ApJS 107, 143
Telles E., 1996, PASP 108, 462
Telles E., Melnick J., Terlevich R., 1997, MNRAS 288, 78
Telles E., Terlevich R., 1997, MNRAS 286, 183
Terlevich R., Melnick J., Masegosa J., Moles M., Copetti M.V.F., 1991, A&AS 91, 285
Thuan T.X., 1983, ApJ 268, 667
Thuan T.X., Izotov Y.I., Lipovetsky V.A., 1996, ApJ 463, 120
Thuan T.X., Izotov Y.I., Lipovetsky V.A., 1997, ApJ 477, 661
Thuan T.X., Martin G.E., 1981, ApJ 247, 823
Van Zee L., Skillman E.D., Salzer J.J., 1998, AJ 116, 1186
Zwicky F., 1971, in Publ. F. Zwicky, Guemligen (BE), Switzerland-388, p. 0